AL/CF-SR-1996-0134

TACTILE FEEDBACK FOR A FORCE-REFLECTING HAPTIC DISPLAY

Christopher J. Hasser

CREW SYSTEMS DIRECTORATE
BIODYNAMICS AND BIOCOMMUNICATION DIVISION
WRIGHT-PATTERSON AFB OH 45433-7022

DECEMBER 1995

Final Report for the Period January 1995 to December 1995

Approved for public release; distribution is unlimited

AIR FORCE MATERIEL COMMAND
WRIGHT-PATTERSON AIR FORCE BASE, OHIO 45433-6573

ARMSTRONG LABORATORY

NOTICES

When US Government drawings, specifications, or other data are used for any purpose other than a definitely related Government procurement operation, the Government thereby incurs no responsibility nor any obligation whatsoever, and the fact that the Government may have formulated, furnished, or in any way supplied the said drawings, specifications, or other data, is not to be regarded by implication or otherwise, as in any manner, licensing the holder or any other person or corporation, or conveying any rights or permission to manufacture, use or sell any patented invention that may in any way be related thereto.

Please do not request copies of this report from the Armstrong Laboratory. Additional copies may be purchased from:

National Technical Information Service
5285 Port Royal Road
Springfield VA 22161

Federal Government agencies and their contractors registered with Defense Technical Information Center should direct requests for copies of this report to:

Defense Technical Information Center
8725 John J. Kingman Rd., STE 0944
Ft Belvoir VA 22060-6218

TECHNICAL REVIEW AND APPROVAL

AL/CF-SR-1996- 0134

The voluntary informed consent of the subjects used in this research was obtained as required by Air Force Instruction 40-402.

This report has been reviewed by the Office of Public Affairs (PA) and is releasable to the National Technical Information Service (NTIS). At NTIS, it will be available to the general public, including foreign nations.

This technical report has been reviewed and is approved for publication.

FOR THE COMMANDER

Thomas J. Moore

THOMAS J. MOORE, Chief
Biodynamics and Biocommunications Division
Crew Systems Directorate
Armstrong Laboratory

REPORT DOCUMENTATION PAGE

Form Approved
OMB No. 0704-0188

1. AGENCY USE ONLY *(Leave blank)*	2. REPORT DATE	3. REPORT TYPE AND DATES COVERED
	December 1995	Final - January 1995 to December 1995

4. TITLE AND SUBTITLE

Tactile Feedback for a Force-Reflecting Haptic Display

5. FUNDING NUMBERS

PE - 61102F
PR - 2300
TA - CB
WU - 51

6. AUTHOR(S)

Christopher J. Hasser

7. PERFORMING ORGANIZATION NAME(S) AND ADDRESS(ES)

Armstrong Laboratory, Crew Systems Directorate
Biodynamics and Biocommunications Division
Human Systems Center
Air Force Materiel Command
Wright-Patterson Air Force Base OH 45433-7901

8. PERFORMING ORGANIZATION REPORT NUMBER

AL/CF-SR-1996-0134

9. SPONSORING/MONITORING AGENCY NAME(S) AND ADDRESS(ES)

10. SPONSORING/MONITORING AGENCY REPORT NUMBER

11. SUPPLEMENTARY NOTES

12a. DISTRIBUTION/AVAILABILITY STATEMENT

Approved for public release; distribution is unlimited

12b. DISTRIBUTION CODE

13. ABSTRACT *(Maximum 200 words)*

This thesis describes the development of custom-built tactile feedback hardware and its integration with an available force-reflecting haptic interface. Design requirements were motivated strongly by the characteristics of the human tactile sense as well as the biomechanical characteristics of the human finger. The work explores the feasibility of various actuators, and selects a small solenoid actuator for application in a closed-loop force control tactile feedback system. An adaptive PI algorithm using continuously variable gain scheduling helps to compensate for nonlinearities in the solenoid actuator. The system demonstrates adequate closed-loop control, but the mass added to the force-reflecting haptic interface proves less than optimal. Design suggestions for future prototypes may reduce the mass added by the tactile feedback hardware by over 30%. The work concludes with recommendations for psychophysical research that will increase understanding of human performance in tasks using haptic feedback devices.

14. SUBJECT TERMS

force reflection
force feedback
tactile feedback
haptic feedback
telerobotics
virtual reality
adaptive controls

15. NUMBER OF PAGES

110

16. PRICE CODE

17. SECURITY CLASSIFICATION OF REPORT	18. SECURITY CLASSIFICATION OF THIS PAGE	19. SECURITY CLASSIFICATION OF ABSTRACT	20. LIMITATION OF ABSTRACT
UNCLASSIFIED	UNCLASSIFIED	UNCLASSIFIED	UNLIMITED

This page intentionally left blank.

SUMMARY

Haptic feedback devices for virtual reality and telerobotics applications reproduce physical sensations to a human operator who interacts with a virtual or remote environment. Motors or other actuators reflect forces of interaction to the arms, hands, and fingers of the user. Tactile feedback devices stimulate the cutaneous tactile sense either to mimic skin touches in the reflected environment or to give a cue to the operator that he or she is encountering virtual forces.

Real manipulation and haptic exploration rely on the seamless integration of the cutaneous tactile and force subcomponents of the sense of touch. Any human interface that replicates only one of these two subcomponents will provide an incomplete sense of "presence" in the reflected environment. The sense of "presence" is defined as the transparency of the operator interface with the reflected environment. The user with a good sense of presence will perceive the reflected environment rather than the interface itself. An imperfect subjective experience will likely lead to degradations in objective measures such as task completion times, errors, forces of interaction, and object discrimination.

This thesis describes the development of custom-built tactile feedback hardware and its integration with an available force-reflecting haptic interface. Design requirements were motivated strongly by the characteristics of the human tactile sense as well as the biomechanical characteristics of the human finger. The work explores the feasibility of various actuators, and selects a small solenoid actuator for application in a closed-loop force control tactile feedback system. An adaptive PI algorithm using continuously variable gain scheduling helps to compensate for nonlinearities in the solenoid actuator. The system demonstrates adequate closed-loop control, but the mass added to the force-reflecting haptic interface proves less than optimal. Design suggestions for future prototypes may reduce the mass added by the tactile feedback hardware by over 30%. The work concludes with recommendations for psychophysical research that will increase understanding of human performance in tasks using haptic feedback devices.

ACKNOWLEDGEMENTS

Many people provided assistance vital to this thesis work. My parents contributed to the values, motivation, and opportunities that brought me to this point. Thanks go particularly to my father for opting not to enter the priesthood. The Air Force provided me with a fantastic undergraduate education that I paid for by working in a job that was more enriching than I could have imagined, while Air Force tuition assistance paid for graduate classes at night. An Air Force Office of Scientific Research grant supported the thesis hardware. My advisor, Prof. Malcolm Daniels, provided able guidance and deserves special thanks for following through on his reassurances to a new graduate student and literally making the controls curriculum happen. The two additional committee members at the University of Dayton, Prof. Dana Rogers and Prof. John Westerkamp, contributed to the quality of this thesis during the editing and defense stages. Prof. Jan Weisenberger helped not only as a committee member, but has been a valued mentor and collaborator for the past four years. Captain (Dr.) Paul Whalen led the Human Sensory Feedback (HSF) for Telepresence Project and encouraged the development of the system. Lieutenant Colonel Peter Lurker played a key role in my assignment to the Armstrong Laboratory. Major Ron Julian, the first leader of the HSF for Telepresence Project, introduced me to tactile feedback, provided an excellent leadership example, and has continued to provide sage advice as a mentor. Dr. Charles Nixon, the chief of the Bioacoustics Village, has created a superb working environment and a great home for the HSF for Telepresence Project. Marvin Roark acted as the software authority of last (and sometimes first) resort. He helped particularly with the interrupt service routine portion of the thesis code. Thomas Massie took time out of his busy production schedule to deliver one-of-a kind hardware within specifications and in the most professional manner. Joe Steuver came to the rescue with tape backups at a crucial moment. Prof. Rob Howe has always been generous with his time and insight. Dr. Mandayam Srinivasan's fingertip modeling efforts offered just the data I was looking for during the design and analysis phases of the thesis. Steve Wilmuth at Lucas offered a suggestion that led to the felt washer to improve the solenoid's behavior. And finally, great

thanks to my wife, Sheila, for her support, many box dinners, tolerance of late nights and weekends in the laboratory, and for letting me talk her into an Australian vacation to top it all off.

Table of Contents

List of Figures

List of Tables

Thesis: Tactile Feedback for a Force-Reflecting Haptic Display

I. INTRODUCTION

Research towards the improvement of telerobotics and virtual reality technology has focused on enabling human operators to achieve a sense of "presence" in the remote or imaginary environment. An operator is able to perceive the environment and act upon it as if he or she were actually there. Generally, enhancing "presence" requires accurate sensing of human inputs or motions, and high fidelity stimulation of the human visual, touch, and auditory senses. Through these means, the operator communicates with a robot slave or some virtual entity. Enhancing sensory feedback has been shown to increase the subjective sense of "presence" and decrease objective task completion times in telerobotic and virtual reality tasks. The term "haptic feedback" is often used to refer to the stimulation of the human sense of touch by telerobotic and virtual reality interface devices.

Webster's II New Riverside University Dictionary defines "haptic" as an adjective meaning "of or pertaining to the sense of touch." The concept of haptic feedback that has developed in the last few years among researchers has a broader than traditional idea of the sense of "touch," but a more specific idea of when it is appropriate to use the term "haptic." Relevant senses include not only the surface (cutaneous) skin sensations normally associated with the touch sense, but also proprioceptive and kinesthetic sensations. Proprioceptors sense muscle forces, while kinesthetic receptors sense the angle and velocity of joint movement. With the inclusion of these senses, it seems intuitive to regard haptic sensations as "active" force, tactile, and motion sensations which change as a result of a person's movements through an environment. With this definition, sensations experienced by a passive user (i.e. tactile array feedback on a stationary finger) would not be considered "haptic." Two classes of haptic feedback devices exist; force feedback devices using motors

or other actuators stimulate the kinesthetic and proprioceptive senses, and tactile feedback devices using small actuators (usually on the fingers) stimulate the cutaneous tactile sense.

In the development of teleoperation and virtual reality interfaces, the sense of touch provided by mechanoreceptors near the human's skin surface has not received as much attention as the other senses. Tactile feedback is vital to achieving a full sense of "presence," and to manipulating the remote or virtual environment with dexterity. Jau et al. built an advanced force-reflecting hand teleoperator system that allows an operator wearing a powered exoskeleton to manipulate tools. Despite the great emphasis that the designers placed on high fidelity force feedback, it became apparent during operational trials that tactile sensing of tool contact and pressure in the hand is essential for good tool manipulation capability (11). Even though considerable research exists on the psychophysiology of human touch, the development of mechanical aids to stimulate this sense realistically has continued to be a serious challenge (31). Tactile feedback requires the development of hardware displays that are lightweight, portable, and suitable for mounting in gloves or other moving strata. Kaczmarek and Shimoga have both conducted thorough reviews on progress to date in developing tactile feedback displays (15, 33).

1.1 Why Force Feedback?

Studies comparing dexterous telemanipulation with force reflection to that without force reflection are difficult to find; however, numerous studies support the value of force feedback in non-dexterous arm telemanipulation tasks. Before considering the use of force reflection in an application, at least three disadvantages must be reckoned with:

- Cost and complexity
- Weight and volume
- Time delay (a potential cause of instability)

Fortunately these disadvantages are not without remedy. Cost and complexity, as well as weight and volume, of systems should be reduced as the technology advances, though force

feedback systems will never be as simple as those without force feedback. The issue of time delay affects only a portion of teleoperation applications. Approaches which use predictive displays may provide some help in coping with time delays. Some control solutions exist which aim to gracefully degrade performance with increasing delay in order to guarantee stability.

Given that the addition of force reflection has a large initial cost, numerous operating advantages in many areas reduce subsequent costs:

- Reduces requirement for position accuracy between master and slave
- Reduces training time
- Reduces dependence on visual feedback for some tasks
- Reduces task completion time
- Reduces grasp forces
- Reduces errors

Force reflection diminishes the need for accuracy between master and slave positions. Being able to feel the environment quickly allows the human operator to adapt to a certain level of inaccuracy. In normal manipulation tasks, people rely more on the senses of touch and force than on position. Training time will likely be reduced due to the intuitive nature of force reflection, and the operator not having to learn to cope with absent or cross-modal sensory information (e.g. visual display of force information). The addition of force feedback will reduce the operator's dependence on visual feedback (22), allowing haptic exploration or groping when vision fails to give sufficient understanding or becomes obscured. Force feedback may also contribute to grasp stability, as the operator will be able to quickly and intuitively adjust grasp forces in response to force changes in the slave environment that are not perceptible through vision.

The literature supports the assertion that force feedback improves performance. Hannaford et al. showed that the addition of force feedback to their tasks reduced completion

time by 30%, sum of squared forces by 86%, and errors by 63%. Patrick et al. compared simple position control to control with either force feedback or simplified feedback via a piezoelectric vibrator (27). Task completion time with the addition of tactile contact (vibration) feedback compared favorably to completion time with force feedback. Both were significantly better than no feedback at all. A key weakness of tactile feedback alone is that the master cannot physically force the operator to stop a motion when the virtual or remote slave encounters an immovable object. The operator may feel his hand and hand master inside the bounds of a remote or virtual object while receiving sensory information based upon the slave's contact with the outside of the object; position registration between master and slave is lost. As task difficulty increases, the gap between force and tactile completion times widens. This shows advantages of force over tactile feedback alone, but suggests that the additional complexity of force feedback must be justified by higher task difficulty. An alternate justification might be an environment where damage is likely or consequences of damage are severe.

Richard et al. used a Rutgers Portable Dextrous Master with Force Feedback to manipulate three virtual objects in a computer simulation: a ball, a spring, and a soda can (28). The authors showed that for the tasks studied, the presence of virtual force feedback reduced learning time by 50% and increased dexterity (as measured by reduction in plastic deformation of the soda can) by 50%. In another study with 64 subjects, Richard et al. showed that after training, force feedback to the hand decreased plastic deformation of a hard virtual ball by 65% from trials with no force feedback (other than cues from a graphics simulation of the ball and slave hand) (29).

1.2 Why Tactile Feedback?

The physiological manipulation studies of Johansson and others, as well as the force-reflecting hand master design and operating experience of Jau et al., suggest tactile feedback is necessary and that force reflection alone cannot provide sufficient sensory feedback (11, 13, 38). In trials with one of the most advanced force-reflecting hand master-slave systems yet

fielded, Jau found that the lack of tactile feedback significantly hampered tool manipulation (11). In addition to giving information about surface details, curvature, and texture, the tactile sense produces a perception of contact location that can be crucial in manipulation. Cutaneous tactile cues can also indicate that an object is slipping within a person's grasp and cause a reflexive tightening of the grasp (13). Only a few force-reflecting projects have included complex tactile feedback (6, 19, 25, 26). The tactile feedback problem equals or exceeds the depth of the force feedback problem (see Kaczmarek and Shimoga for excellent reviews (15, 33)).

The addition of tactile feedback to a force feedback device adds mass and complexity to a class of systems that already exists near the boundary of feasibility. The fact that both research areas can be cost and labor intensive also helps to explain why few efforts have attempted to add tactile feedback to force-reflecting interfaces. The first dual tactile/force systems that actually work and are followed up by published experiments with some generalizability will involve simplification of at least one of the systems. Kontarinis, Howe, et al. have added complex tactile feedback to a simple (planar) high-fidelity finger master-slave system. The present thesis work will add a simple one-actuator tactile device to the PHANToM™ haptic interface (which reflects forces in three dimensions rather than two). Follow-on work will add shape-memory alloy (SMA) driven tactile arrays similar to those of Kontarinis and Howe.

1.3 The PHANToM™ Force-Reflecting Haptic Interface

The PHANToM™ Force-Reflecting Haptic Interface is a three degree-of-freedom high-fidelity device for displaying forces to an operator's hand. The operator can insert his or her finger into a thimble that is attached via a gimbal to a small, desktop three-link mechanism, or can use a stylus which attaches to the gimbal. Either attachment gives an extremely high bandwidth force feedback signal to the hand when the operator moves into a virtual fixture (surface generated in software.) A photograph of the PHANToM™ with a thimble terminus appears in Figure 1. Appendix A contains specifications for the PHANToM™. When the

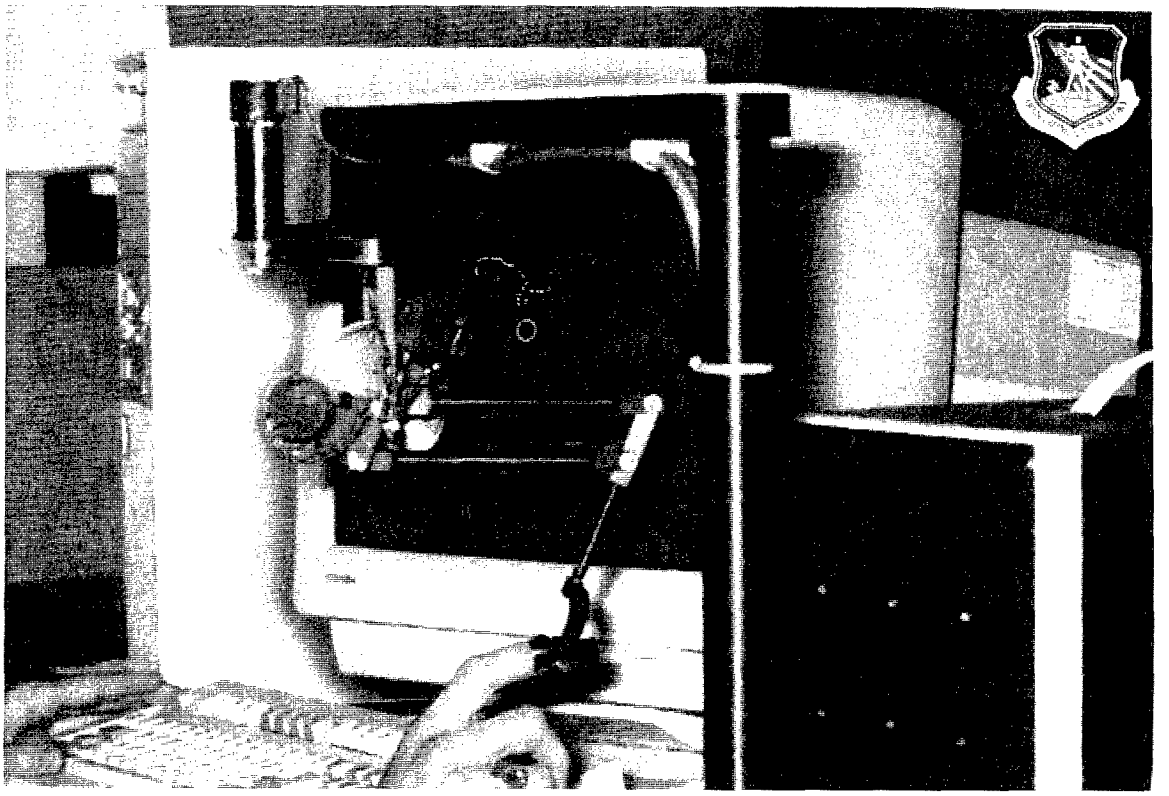

Figure 1. The PHANToM™ Force-Reflecting Haptic Interface

thesis project began, no other commercially available system had the fidelity and bandwidth of this system. The PHANToM™ takes advantage of the fact that many interactions can be modeled as point contacts, where forces are relevant but torques are not. Such interactions as a pencil contacting a surface or a finger touching a pushbutton serve as examples. In these contacts, the tool (pencil, etc.) or finger is constrained by Cartesian forces but can move freely in pitch, roll and yaw. The three-link arrangement of the PHANToM™ allows Cartesian force reflection and the thimble gimbal allows free movement in pitch, roll, and yaw. The fact that the PHANToM™ designer did not attempt to apply forces to the pitch, roll, and yaw degrees of freedom markedly reduced the complexity of the design. Actuating orientation degrees of freedom would require heavy actuators at the end point of the device, or complicated transmission systems to transfer power to the gimbal from actuators closer

to the base. Avoidance of orientation actuation led to a low-inertia, high-bandwidth design that retained a substantial ability to model general force-reflecting virtual environments.

1.4 Thesis Concept

Given a high-fidelity force-reflecting haptic interface, this effort will attempt to enhance it with the addition of a single-element tactile feedback stimulator. The stimulator will be capable of both steady state and vibratory forces. Two main challenges exist:

- To develop tactile feedback hardware that results in a net gain in capability
- To develop an elegant software driver for the hardware that gives a robust and intuitive percept of the reflected environment

The hardware challenge requires not just a well-implemented actuator system with adequate controllable output. It also requires a system whose added mass does not degrade the dynamic performance of the force-reflecting haptic interface so much that the additional hardware causes a net loss in system capability. Since a key to the success of the PHANToM™ is the *avoidance* of structural mass at its end point, much of the current effort's risk arises from this constraint.

The rendering of haptic environments in software has similarities to the rendering of computer graphics, both technologically and historically. Software algorithms for rendering haptic environments will borrow many techniques from the arena of computer graphics. Algorithms for collision detection must be extended, and new algorithms for characteristics such as hardness must be developed. Historically, computer graphics hardware progressed from simple vector graphics machines to immensely powerful graphics engines over a period of a few decades. Haptic rendering software is still struggling to emerge from the vector/cartoon stage. Most haptic demonstration programs use simple shapes like cubes and spheres that may move but do not change shape (other than yielding to pressure from a finger or hand). Complex objects or those that can be changed (e.g. cut with a virtual scalpel) demand much higher levels of sophistication.

The present thesis does not involve the development of haptic rendering algorithms, but an awareness of their complexity leads to a desire to keep things as simple as possible with the tactile driver software. Software developed to drive tactile feedback hardware should be elegant and compatible with force-reflecting hardware driver algorithms. An optimal tactile feedback algorithm will impose few or no additional demands on the haptic rendering software. The cost of implementation would increase considerably if haptic software had to store tactile as well as force characteristics for every segment of every object in the synthetic environment. Sections 4.6 and 5.6 present a tactile driver algorithm that meets these demands.

II. TACTILE PERCEPTION

This chapter contains a very brief introduction to relevant information about the human tactile pressure and vibration sense in glabrous (non-hairy) skin (excluding any mention of pain and thermal senses). A cursory glance at the complexity of the tactile sense and the simplicity of current stimulation methods will reveal the crudeness of the available stimulation technology. Glib predictions in the popular and even scientific literature about the potential of tactile feedback devices should be regarded with caution. For a more thorough coverage of tactile perception, the reader should consult the following works. Sherrick and Cholewiak offer a review of the mechanisms of cutaneous sensitivity (32). Loomis and Lederman cover the psychophysical aspects of tactual perception (21). Johansson and Westling published research on how tactile nerve signals influence adaptive muscular responses in precision grasps (13, 38). Moore's review in 1966 presents an interesting historical snapshot of a time when currently accepted theories of tactile sensitivity where beginning to take hold against now-rejected assertions of earlier investigators (23).

2.1 Anatomy and Physiology

At least four neural mechanoreceptors in the human fingertip enable cutaneous tactile sensations to be felt through afferent nerve fibers that carry the sensations to higher levels of the nervous system. These mechanoreceptors lie at the ends of nerve fibers and possess different anatomical characteristics that are believed to influence the type of stimulus they relay into the nervous system (Figure 2). Through a process called microneurography, tiny electrodes placed in afferent nerve fibers ascending the arm have been used to record electrical impulses originating from the mechanoreceptors. The afferent nerve fibers have been classified into four groups based upon the behavior of their measured impulses in response to mechanical stimuli at the fingertip.

Through a combination of dissection and comparison of the afferent behaviors to the anatomical characteristics and locations of the mechanoreceptors, a connection between

Table 1. Tactile Mechanoreceptors, Afferent Nerves, and Frequency Ranges

Mechanoreceptor	Afferent Nerve Type	Sensitive Frequency Range (12)	Receptive Field [mm^2] (15) *(median)*
Pacinian corpuscle	FAII (RAII, PC)	> 64 Hz	10-1000 *(101)*
Meissner's corpuscle	FAI (RAI, RA)	8-64 Hz	1-100 *(12.6)*
Ruffini ending	SAII	< 8 Hz	10-500 *(59)*
Merkel's cells	SAI	2-32 Hz	2-100 *(11.0)*

FA = fast adapting; RA = rapidly adapting; PC = Pacinian; SA = slowly adapting

each of the four mechanoreceptors and a particular type of afferent nerve fiber has been implicated. Table 1 associates each mechanoreceptor with an afferent nerve type and lists the range of frequency sensitivity and receptive field size for that type. Table 1 and Figure 2 show that mechanoreceptors with small receptive fields lie close to the skin surface, and those sensitive to stimulation on wider areas of the skin surface lie farther from it.

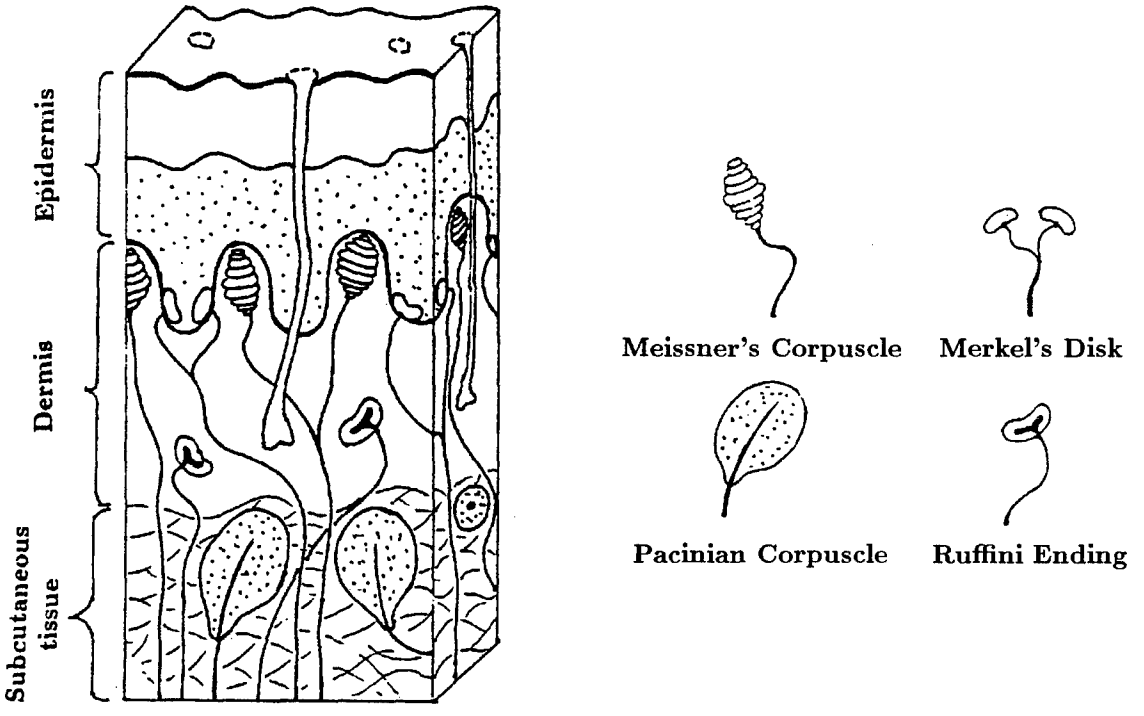

Figure 2. Touch Receptors in the Glabrous Skin of the Human Hand (from Shimoga (34))

Human skin is composed of underlying subcutaneous tissue (fatty layer), the dermis, and the epidermis (outer skin layer). The upper layer of the subcutaneous tissue holds the **Pacinian corpuscles** just under the dermis. Only the Pacinian corpuscles have a single dedicated nerve fiber for each mechanoreceptor. They can reach sizes of 1-4 mm and typically lie 2-3 mm from the skin surface. Fluid-filled **Meissner's corpuscles** are located in the papillary ridges of the dermis, just under the epidermis. They may accept up to nine separate nerves, which may branch to connect with neighboring corpuscles. **Ruffini endings** are spindle-shaped capsules approximately 0.5-2 mm in length that rest within the dermis. Ruffini endings are associated with the SAII afferent nerves, the only afferents that have been shown to be sensitive to lateral skin stretch as well as indentation (32). **Merkel's disks** rest at the bottom of the epidermis, just above the dermis. The encapsulation of the two corpuscles associated with rapidly-adapting afferents is believed to provide high-pass filtering so that they remain unaffected by steady force displacements common in grasping.

In an excellent analysis of the roles of the mechanoreceptors in tactual form (pattern) and texture perception, Johnson and Hsiao present the following working hypothesis for the roles of the SAI, RA [FAI], and PC [FAII] systems (14):

> The *SAI system* is the primary spatial system and is responsible for tactual form and roughness perception when the fingers contact a surface directly and for the perception of external events through the distribution of forces across the skin surface. The *PC [FA II] system* is responsible for the perception of external events that are manifested through transmitted high-frequency vibrations. The *RA [FAI] system* has a lower spatial acuity than the SAI system but a higher sensitivity to local vibration and is responsible for the detection and representation of localized movement between skin and a surface as well as for surface form and texture when surface variation is too small to engage the SAI system.

Perhaps some of the most interesting tactile research from an engineering and robotics perspective has been performed by Johansson. In one effort, Johansson measured thumb and forefinger grip forces on objects with different surface coefficients of friction as they were lifted and held in the air (13). Johansson used microneurography to measure responses of the tactile afferent nerve fibers during the task, showing that the nerves registered slip

activity that led to a reflexive increase in the grip force. This work demonstrates closed-loop grip control based upon human force sensor and slip sensor information in a way that is intuitively complete to the controls or robotics engineer. Johansson concluded that the FAI (RA) and SAI afferents were the primary contributors to slip sensing, and that they demonstrated an ability to record localized microslip activity. The Type I afferents correspond to the Meissner and Merkel mechanoreceptors (Table 1) that lie close to the surface of the skin (Figure 2). The FAII afferents (corresponding to the Pacinian corpuscles) seem better suited to detecting global vibration information, such as contact with objects or collisions between a tool and the environment.

2.2 Relevance to the Current Work

2.2.1 Form Perception. As stated above, the perception of forms (patterns) such as embossed letters, Braille dot patterns, and other surface shapes relies primarily on the spatial discrimination capability of the SAI afferents (associated with Merkel's disks). Perception of patterns relies on simultaneous information from many SAI receptors. While the current hardware may excite SAI receptors, with only one blunt probe conventional shape perception will be impossible. Users may be able to construct integrated images of a shape as they sweep the probe over it repeatedly, but this amounts to a tactile display with a field of view of one element. Unpublished results obtained by Weisenberger and Hasser showed that decreasing tactile feedback array size from nine elements to four elements or to one element severely handicapped users' abilities to discriminate tactile patterns.

2.2.2 Texture Perception. Johnson and Hsiao report that at least two features within the category of the percept "texture" can be analyzed on a continuum of intensity and permit "greater than," "less than," comparisons. These features are hard versus soft and rough versus smooth. In work described in section 3.2, Wellman and Howe performed work that indicates that tactile vibration information of a type possible with the current

system can be used to discriminate hardness of surfaces in virtual and remote environments (37).

The perception of roughness is especially interesting, since it has been attributed both to the spatial tactile sense and the non-spatial tactile sense. Any perceptional ability for roughness that relies on the spatial sense will be lost with the current device, while any roughness perception that does not rely on the spatial tactile sense may be retained. With respect to texture perception, the current device is analogous in some ways to perceiving the environment through a tool (e.g. a metal rod swept across a rough surface).

Johnson and Hsiao conclude that the SAI spatial mechanism plays a leading role in roughness perception, but under special circumstances other afferents play key roles instead (14). PC receptors respond weakly to textural features such as dot spacing, but Lamotte and Srinivasan (cited in (14)) found that only PC receptors responded to finely etched dot patterns and gratings 0.1 microns above the background. LaMotte (also cited in (14)), worked with machined asperities 2 microns high to which only RA afferents responded. Clearly, non-spatial cues play a role in roughness perception and will be relevant to the current device, though its ability to improve upon the roughness perception possible with a non-tactile force-reflecting interface such as the originally-equipped PHANToM™ is uncertain.

III. PREVIOUS WORK

There are few reports of direct tactile feedback in telerobotics. Browse and McDonald compared visual presentations of tactile data combined with visual scene image to simple visual scene image alone, for the ability of subjects to predict a stable grasp on various block-style objects with a parallel jaw gripper (2). No experimentation with direct tactile feedback to the subject's fingers was included. The authors concluded that visual presentation of tactile data increased the chances that a subject would accurately predict stable or unstable grasp for their experimental setup.

Virtual research with haptic feedback commonly concentrates on tactile feedback or force feedback, but not both. One exception is the Hand Exoskeleton Haptic Display (HEHD), a Small Business Innovation Research (SBIR) project for the Human Sensory Feedback for Telepresence Project at the Armstrong Laboratory, conducted by EXOS Inc. (3). HEHD incorporates force-reflecting hand exoskeleton technology developed under NASA SBIR projects, and adds slip feedback provided by rotating cylinders powered by miniature dc servomotors. Numerous psychophysical experiments were carried out to support the development of the prototype and to develop control strategies for the slip feedback. The efforts of Howe, et al. are another exception. Howe and his students have mated both tactile feedback arrays and vibration feedback devices to force-reflecting interfaces in work described later in this chapter (10, 18, 19).

3.1 Tactile Array Feedback

While the issues of tactile array feedback differ somewhat from those of a single-element actuator such as the current device, array feedback systems constitute the majority of the previous body of work. Since the current system can be viewed as a research stepping-stone, and many useful applications will incorporate array feedback, the subject will be covered here.

Bliss et al. constructed two tactile feedback systems (1). A 24-element airjet system fed tactile signals to each of the 24 phalanges on a human hand (excluding the thumb). The second system consisted of a 4×8 array of piezoelectric bimorphs, spaced on 0.1-inch centers, which was used to feed back tactile information from an on-off tactile sensor with similar resolution. The sensor was placed on a pair of gripper tongs, and a master-slave telerobotic system was used to demonstrate performance improvement with the tactile feedback array. The operator's finger is centered over the actuator array. With 12 rows on 0.1-inch centers, the array is approximately 1.2 inches long; the array extends beyond the distal phalange (finger pad) of the index finger, partially onto the medial phalange.

Bliss showed that tactile array feedback slightly reduced task completion times (by about 7%) for a complex latch-removal task, but significantly increased the percentage of tasks completed successfully (17-40% improvement). Tactile feedback became even more important when vision was obscured to varying degrees. Bliss also found that the value of tactile feedback depended on the novelty of the task, suggesting that tactile feedback is important for exploratory work where the tasks are highly variable or perhaps unknown ahead of time. Bliss' results showed that when the object is fragile, or hard to find, or requires accurate positioning to be picked up, the tactile feedback system increases efficiency.

Kontarinis and Howe have constructed a 9-pin SMA-actuated tactile feedback array, with stimulators spaced 2 mm apart (17). They have mounted the device to a pair of planar two-degree-of-freedom finger master controllers, with the tactile feedback arrays perpendicular to the plane of motion (9). The master-slave testbed also has an identical pair of slave manipulators with tactile array sensors, which has enabled the simulation of two-finger planar telemanipulation with tactile feedback (19).

The SMA tactile array feedback device developed by Kontarinis has been paired with a tactile array sensor and applied to tumor and artery location tasks (10). Investigators placed the tactile sensor over a human's radial artery and relayed the pulsatile sensation to the SMA feedback array. They also showed that with tactile shape feedback subjects could

use the teleoperated system to locate a 4 mm diameter hard rubber "tumor" embedded 5 mm below the surface of a block of foam within 3 mm of its correct location 95% of the time. Without tactile shape feedback, the mean error was 13 mm.

Oomichi et al. constructed a master-slave arm and hand telemanipulator system (24). The hand master is a full exoskeleton, with what appears to be single-element pneumatically-driven tactile feedback elements on each fingertip. More specific information on the tactile feedback mechanism or its contributions to assembly/disassembly operations carried out with the system was not available.

3.2 Feedback of Vibration Sensations

Numerous investigators have used vibration feedback as a substitute for force feedback, seeking to make the user feel as if he or she has contacted an object in the environment without the cost and stability concerns of force-reflection systems. This approach uses vibration feedback devices driven by force sensors at the teleoperated slave or force computations in the virtual environment. This section discusses the use of vibratory actuators such as voice coils to reproduce *vibration* rather than force sensations. Either an accelerometer signal or a software-generated vibration signal drives the vibration feedback actuator. Since the tactile stimulator developed in this thesis can easily act as a vibration feedback actuator, the work discussed below has a direct bearing on its potential applications.

Kontarinis and Howe use binary vibration feedback to reduce overforce errors in a two-target tapping task (16). For a teleoperated tapping task, successful taps increased by an average factor of 1.8 when a solenoid provided binary vibration information (a short vibration burst) indicating that the probe had just touched the target.

Kontarinis and Howe also introduced a more capable vibration feedback mechanism that has been attached to their two-fingered teleoperation system (18). Each of the two master devices (one for the forefinger and one for the thumb) has been fitted with modified speakers (with the paper cone and mounting bracket removed) so that they can present

vibration information to the user as well as force feedback. The speaker coils vibrate the fingertip handles of the master controller. Human subjects used the system in three experiments: detecting worn bearings by feeling for vibrations, puncturing a membrane, and inserting a peg in a slot. Results showed that the addition of simple vibration feedback had significant positive effects for the bearing examination task, significant effects for the membrane puncturing task (but less so than for the bearing examination task), and no significant effect for the peg-in-slot task. Despite the lack of a significant effect on performance in the peg-in-slot task, subjects reported that the addition of vibration feedback increased their sense of presence and that they preferred the system with vibration feedback as well as force feedback.

Wellman and Howe describe further work with Howe's voice coil vibration feedback system, measuring accelerometer signals from tapping on surfaces of various hardness and characterizing these signals as damped sinusoids (37). Human subjects were first asked to conduct pairwise discriminations between surfaces with five different hardnesses. They could do this with very good success. After that, the experimenters used damped sinusoidal signals to simulate tapping in a virtual environment. Subjects could discriminate well in the virtual environment, but not as well as in the teleoperated test where the vibration feedback was driven by actual accelerometer signals.

IV. DESIGN

This chapter presents the evolution of a design intended to meet the hardware and software challenges outlined in section 1.4. It covers the two major subcomponents of the design: the orientation-sensing gimbal and the tactile actuator system. It also covers a test stand constructed to test control algorithms and gather data prior to final design implementation. Discussions related to the test stand will appear in this chapter, and any discussions of work performed with the tactile actuator thimble will appear in Chapter V. A discussion of software representation design issues appears at the end of this chapter. Chapter V describes details of the implemented software algorithm.

4.1 Mass Loading of PHANToM™

One of the major advantages of the PHANToM™ over other force-reflecting devices is its extremely low inertia, with an effective mass at the tip of 50-100 grams. The proposed encoders, enlarged gimbal, and tactile feedback actuator will all have masses that are significant with respect to the original 50-100 gram effective mass. In an effort to roughly gauge the effect of additional mass, three representative PHANToM™ demonstration programs were explored using additional masses at the tip of 60 grams and 120 grams. The masses where counterbalanced with masses attached to the PHANToM™ motors. The demonstration programs contained virtual environments with spheres, buttons, and textured surfaces. The PHANToM™'s performance was subjectively rated based upon the perceived crispness of hard surfaces and salience of fine surface details. Performance with a 120 gram mass at the tip was sufficiently degraded to warrant the selection of 120 grams as the maximum allowable mass of additional hardware. If possible, the hardware should be substantially lighter than 120 grams.

An objective measure of the effects of additional mass would offer much more information than a few anecdotal trials. Anecdotal information may be sufficient to set a target for an initial prototype, but future design changes involving the addition or subtraction of mass

should be informed by a quantitative understanding of their impact. A study currently underway at the Human Sensory Feedback for Telepresence Project involves a PHANToM™ programmed to present subjects with a virtual tapping task (Fitts' Law task) that requires both speed and accuracy. Preliminary results indicate that a virtual 100 gram mass on the subjects' fingertips causes a statistically significant degradation in subject performance. Future experiments with multiple values for mass should provide more specific information about the effects of varying mass. This experiment provides information only about mass effects on a Fitts' Law dexterity task. These results will not necessarily be generalizable to different tasks such as perception of surface texture or object manipulation.

4.2 Gimbal Design

The original PHANToM™ gimbal is made of glass-filled delrin, with three stainless steel bearings. It has a mass of 18 grams. Accommodation of a tactile feedback device requires a larger gimbal with clearance for the tactile stimulator structure and with angle sensors for pitch, roll, and yaw. Both modifications would increase the mass of the gimbal.

A survey of orientation-sensing gimbals designed for other customers by SensAble Devices, the PHANToM™ manufacturer, revealed that no previous designs would meet the needs of this effort. Two options were to modify a 90 gram gimbal design that used very accurate but heavy encoders, or to modify a 50 gram design that used lighter but less accurate encoders. The suitability of the modified light gimbal depends on the adequacy of the lower-resolution encoders.

A comparison of the lighter but less accurate Oak-Grigsby encoder resolution to the just noticeable difference (JND) of human joint angle sensing will test the adequacy of the encoder resolution. Fingertip pitch corresponds to finger flexion and wrist flexion. Fingertip roll corresponds to wrist rotation. Fingertip yaw corresponds to finger abduction/adduction and wrist yaw. Tan et al. report that the the finger flexion angle JND in human joint space is 2-2.5 degrees for the metacarpal-phalangeal (MCP) and proximal interphalangeal (PIP)

joints, and is relatively independent of the starting joint position (36). The same reference reports the wrist angle JND as 2 degrees. The 512-count Oak-Grigsby encoders have an angle resolution of 0.7 degrees, nearly three times better than the human's angle sensing resolution in the relevant joints.

4.3 Tactile Actuator Selection

The addition of tactile feedback requires an actuator capable of adequate force with a mass low enough to avoid compromising the PHANToM™'s dynamic performance. To represent hard surfaces, the stiffness of the actuator system needs to be higher than that of the fingertip. Also, adequate representation of dynamic environments requires a high bandwidth.

Gulati's investigation of the mechanical properties of the human fingertip using a tactile stimulator provides sufficient information to estimate the maximum force and range of motion required for this application (7). Gulati used three probes: a point probe, and flat plate probe, and a circular indentor with a diameter of 6.35 mm. Gulati's 6.35 mm circular probe has the same diameter as the probes manufactured for the present work, and is believed to be identical to the flat 6.35 mm circular probe of the present work. Gulati measured the steady-state force vs. displacement for the circular indentor on the fingertips of five subjects. His results for this case appear in Figure 3.

The average maximum steady state force at the maximum measured displacement of 3 mm was 1.0 N. Consultation with Gulati and other colleagues suggests that a 4 mm indentation might be a good maximum design goal; indentation to any greater depth is likely to be impractical and painful. Using Gulati's data to loosely extrapolate beyond 3 mm, this author chose 2 N (200 g) as a design goal for maximum tactor force.

4.3.1 Actuation Methods Considered. Four actuation options were considered: an electric motor with threaded screw reducer, shape-memory alloy (SMA) wires, pneumatic pistons, and solenoids. An electric motor was rejected mostly because of the high parts

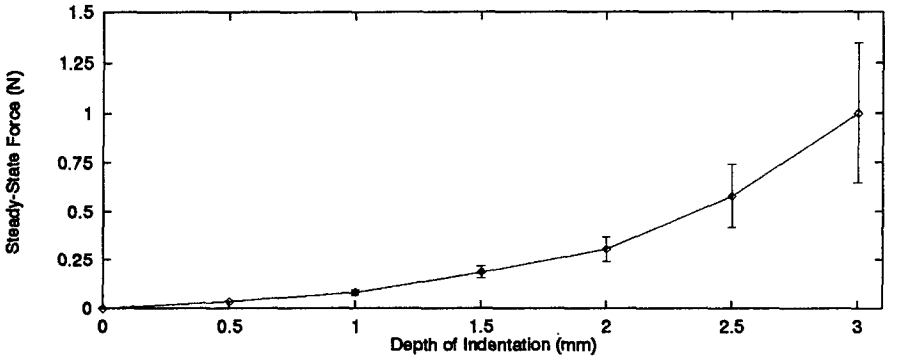

Figure 3. Average Steady-State Force versus Depth with Standard Dev. (Circular Probe)

count and complexity, as well as concerns about backlash and bandwidth. SMA wires constrict when heated, usually by passing current through them. They have extremely high power-to-mass ratios, but extremely low efficiency, and low bandwidth. SMA wires can be difficult to control (17). A pneumatic actuator would require supply tubing to be attached to the end of the PHANToM™ and high-tolerance machining to fabricate a custom tactile feedback actuator. Pneumatics would also require a cumbersome powerplant (tank or compressor) in addition to the electrical amplifiers already used for the PHANToM™ motors.

Solenoids were initially rejected due to their nonlinearity and the author's perception that they could not produce high enough forces. A survey of available solenoids revealed a small model from Lucas Ledex that could produce the required forces. The nonlinearity could potentially be ignored with closed loop force control, or linearized with a position sensor and solenoid model. The solenoid could also be proportionally controlled using an extra PHANToM™ servo amplifier, taking advantage of a robust existing hardware and software interface.

4.3.2 Solenoid Actuation. Solenoid actuation has the advantage of a significantly lower mechanical parts count when compared to other methods. The solenoid itself consists of only two parts: a body, and a plunger. Since a solenoid is a declining air gap magnetic

actuator, its force capability varies nonlinearly with displacement of the plunger. When the plunger is far away from its seated (fully actuated position), forces can be relatively low. When the plunger is close to fully seated, the force gradient can be quite steep, and the plunger difficult to proportionally control.

Luckily, with a push-style plunger, low forces with the plunger away from its seat will occur when the contactor tip first touches the user's finger. As the solenoid drives the contactor tip farther against the user's finger, the plunger will get closer to the seat, increasing the force capability (less current required to generate a given force). This arrangement makes it more likely that a solenoid capable of the required forces throughout the displacement range can be found, and reduces the power (and thus the significant waste heat) that must be delivered to the solenoid.

Whether position or force control is used, linearization of the solenoid would be helpful. If a force sensor closed a force-control loop, linearization of the force control based upon a model of the solenoid and measured displacement will allow for a linear, time-invariant system (the commanded current input vs. force output relationship will not change with displacement). With a good force sensor and a high bandwidth system, control might be adequate even neglecting linearization. The cost of this approach to linearization is the overhead of including a position sensor in addition to a force sensor, as well as additional computation time in the servo loop.

Another scenario exists: a tactile feedback system with a position sensor but no force sensor. In this scenario, the system can be controlled in two different ways. First, the system can obviously use closed-loop position control. Second, the system might implement open-loop force control, using a linearization model of the solenoid dependent on measured displacement.

4.4 Tactile Stimulator Test Stand and Sensors

A test stand (Figure 4) aided in the early testing of control algorithms and the design of the tactile stimulator thimble. It allowed the evaluation of both position and force sensors, and was also used for linearization studies of the solenoid current/force curve based upon a knowledge of the plunger position.

Whether to control tactile stimulators with force control or position control remains an open question, and so obviously does the choice of sensor to close the control loop. In fact, closed-loop control on tactile stimulators has been a luxury, and many investigators have done without (1, 8, 17). Recently, Howe and Kontarinis have included infrared LED's and photodiodes in their SMA design to implement closed-loop position control. Given that the question remains open, it would be desirable to have both position and force sensors in a research device to obtain data and to allow either position or force control. Since a single tactor arrangement does not have the space or cost constraints of a large array, it seemed reasonable to attempt a prototype with both force and position sensing.

4.4.1 Force Sensors. The application requires a force sensor that can be placed in-line along the movement axis of the tactile stimulator. A very thin force sensor would reduce the overall length of the tactile stimulator and make it easier to fit it into the restricted gimbal space. Furthermore, the force sensor needs to have a good signal-to-noise ratio, be as light as possible, and be easy to integrate into the overall design.

A load cell with a 1000 g capacity was the most appropriate stock model for the anticipated 0-200 g operating range, offering a comfortable safety margin to reduce the likelihood of damage to the delicate load cell. The test stand uses a 1000 g Cooper Model LPM 510 button load cell with a 9.65 mm (0.38 in.) diameter and 3.30 mm (0.13 in.) thickness. The tactile feedback thimble uses a 1000 g Sensotec Model D donut semiconductor load cell with outer diameter 12.7 mm (0.50 in.), inner diameter 2.54 mm (0.10 in.), and thickness 3.81 mm (0.15 in.). Both models have non-linearity, hysteresis, and non-repeatability ratings better than 0.5% full scale (5 grams).

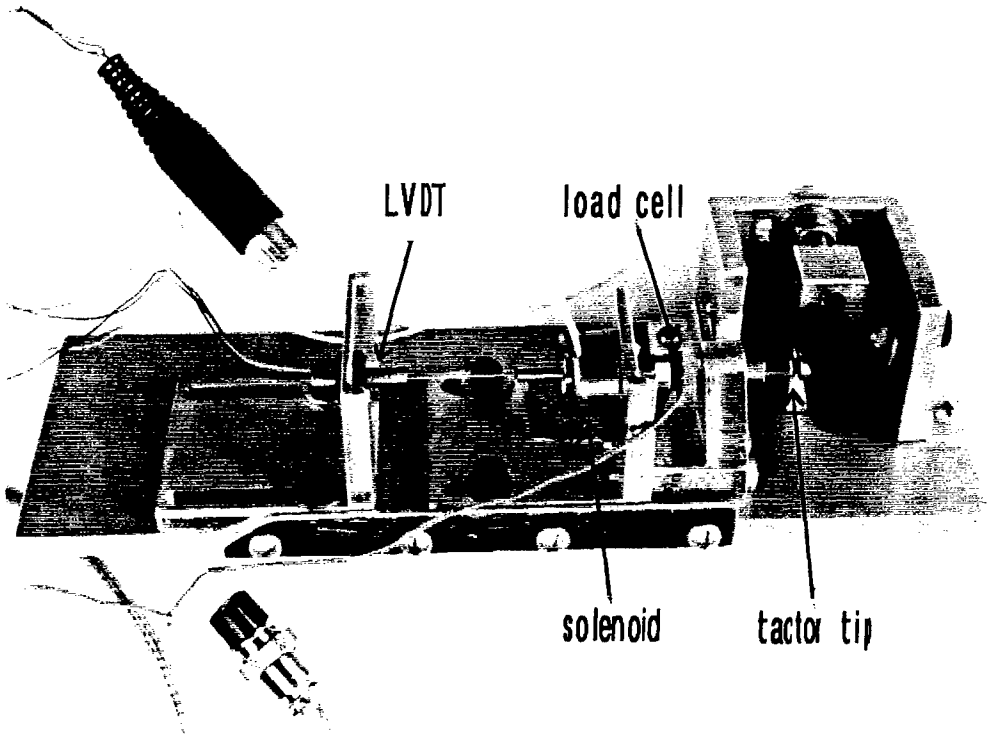

Figure 4. Test Stand with Actuator, Position Sensor, and Force Sensor

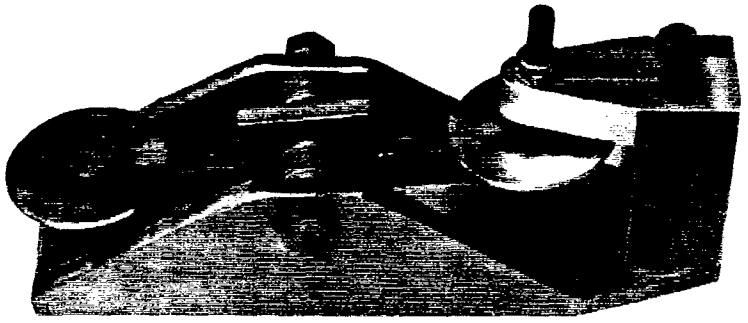

Figure 5. Load Cell Calibration Scale

The load cells were calibrated using the scale pictured in Figure 5 and a set of metric reference masses. The scale has a friction of 1-2 grams, determined by the fact that a 1 gram mass placed on one side of the scale will not cause it to sink all the way down, while a 2 gram mass will. Either one of the load cells can be screw-mounted to the underside of the scale's overhanging arm, while masses are placed on the other side. With a 1000 gram mass on the balance, an oscilloscope on the load cell output, and the coincidental arrival of Dr. Whalen's energetic three-year old child in the laboratory, this setup revealed itself to be a good amplifier of local seismographic activity.

4.4.2 Position Sensor. A Linear Variable Differential Transformer (LVDT) was chosen as a position sensor. The LVDT is reliable, accurate, small, and compatible with LVDT controllers that were already available in the laboratory. The Lucas Schaevitz 099 XS-B LVDT used for this system has a measurement range of 5 mm (0.2 in.). It measures 4.8 mm (0.19 in.) in diameter and 19 mm (0.75 in.) long. A Lucas Schaevitz MP-2000 LVDT signal processor outputs an analog voltage between about -3 V and +3 V over the displacement range of the 099 XS-B LVDT.

4.5 Human Pressure Perception

An ideal haptic feedback device possesses enough fidelity to "fool" the human's senses without wasting effort on fidelity that lies below the human's perceptual limits. In some cases, keen perceptual capabilities will place unrelenting pressure on system designers. Other cases will be considerably more forgiving. The requirement for force control accuracy is likely to be more forgiving. In order to design a control system that can control forces more accurately than humans can perceive them, the force controller must be more accurate than the human's just-noticeable difference (JND) for that particular situation.

Tan et al. measured pressure JND at the elbow (dorsal and volar) and at the wrist (36). Investigators tested three contact areas, 1.27 cm^2, 5.06 cm^2, and 20.27 cm^2. The contact area of the flat probe used in this thesis work is only 0.317 cm^2, the area of the face of a 1/4 inch diameter cylinder. The results of Tan et al. indicate that JND gets larger for smaller contact areas, from an average of 3.7% for a 20.27 cm^2 contact area to an average of 15.6% for a 1.27 cm^2 contact area.

Tan et al. note that pressure JND seems to be relatively independent of test site (though they did not include the index fingertip). They go on to state that pressure JND seems to relate directly to the perimeter of the contact area, rather than the size of the area. Stated in these terms, the JND is 0.06-0.09 N per centimeter of contact perimeter,

regardless of area. The authors cite the extreme sensitivity of the tactile system to pressure gradients as the likely explanation for this perimeter-dependent relationship.

Estimating based upon the results of Tan et al., the force JND for this application, assuming a 0.635 cm (1/4 in.) diameter flat contact plate, would be:

$$\pi(0.625cm)(0.06N/cm) < F_{JND} < \pi(0.625cm)(0.09N/cm) \quad (1)$$

$$0.12N < F_{JND} < 0.18N \quad (2)$$

The equivalent mass JND would be 12-18 grams. If the actuator and sensor design above can apply a commanded force to the fingertip within specifications, the device will still require software that interprets activity in the virtual environment and translates that activity into appropriate command signals for the tactile stimulator.

4.6 Software Representation of Tactile Probe in a Virtual Environment

The demonstration programs supplied with the PHANToM™ model its end point as a single point in virtual space (see Figure 6). When testing for contact with virtual objects, the software determines whether this single point has violated a virtual surface. The single point is infinitely small in theory, but in practice is a sphere with a diameter about the size of a displacement corresponding to a single encoder tick. The user experiences the environment as if he or she where holding on to and controlling the head of a pin moving about in virtual space.

A number of facts immediately become apparent. The virtual PHANToM™ end point can fit into very small spaces; the point-model allows exceptionally high spatial resolution. The user experiences the task more like he or she would through a fine-tipped tool than through a blunt finger. This makes PHANToM™ operation with the stylus very natural. The operator sees the pen-like stylus connected to the gimbal with the stylus tip coincident

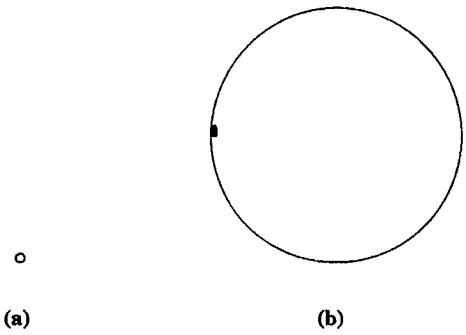

Figure 6. Virtual Representation of the PHANToM™ Probe as a Single Point (a) and as a Sphere with Tactile Point Sensitivity (b)

with the center of rotation of the gimbal. The user can intuitively imagine the stylus tip being a small point in virtual space.

The exact virtual-real world correspondence is lost for the case where the user's finger is inserted into a thimble attached to the gimbal. In real space, the user probes with a blunt fingertip 1.8 cm or so in diameter. In virtual space, this probe is a tiny point. The user can push his finger into tiny crevices that couldn't be entered by a real finger and can experience fine details not apparent through a blunt probe.

One consequence of decreasing point size is decreased field of view. Field of view to the tactile sense is just like field of view to the visual sense. When placed against a flat surface, the fingertip has a two-dimensional field of view equal to the finger area in contact with the flat surface. In real space, the thimble-equipped PHANToM™ is analogous to a thimble with a pin fixed in place and protruding out from its exterior surface; the user can experience "infinitely" small details with an "infinitely" small field of view. While this arrangement allows the ultra-high resolution that is an often-mentioned characteristic of the PHANToM™, decreasing the field of view can have serious consequences. Many tactile perception tasks require a significant field of view; for example, reading a Braille letter or determining the orientation of an edge contact. This is so difficult and time consuming with a single-point model that it is not feasible in many situations. Actively searching for objects also requires a large field of view. Imagine trying to find a plane in the sky while

looking through a pinhole in a piece of cardboard held at arms length. The same holds for the haptic senses. Searching for a small object in a virtual space could take a very long time. The user can search an area or volume for small objects much quicker with a blunt probe than with a fine one.

It seems natural to consider modelling the PHANToM™ tip as a sphere in virtual space, with a diameter equal to that of the fingertip. The PHANToM™ is a force-reflecting haptic interface, and in real life the mechanoreceptors that code force stimuli receive their information from a probe that is fingertip-sized (assuming that only fingertip contact occurs). In real-life fingertip contact, very fine details are coded by tactile mechanoreceptors at the fingertip skin surface, not the kinesthetic force mechanoreceptors as when the user experiences them through the PHANToM™.

By modelling the virtual fingertip as a sphere rather than a point, we might make the experience more "real," but we would lose the ability to perceive small details. How could we retain our newly acquired field of view and still have the ability to sense fine details? By advancing our feedback device to mimic reality more fully with the addition of a stimulator that touches the fingertip of the user. This stimulator could be linked to an imaginary "touch sensor" in virtual space that is modelled as a point on the virtual sphere representing the fingertip. One could mimic this effect by placing a subject's finger in a thimble that has a hole drilled in it, with a short piece of wire poking out of the hole, free to move in and out against the finger as fine details where encountered.

By using two different (but related) senses, the kinesthetic force sense and the surface tactile sense, we could give the user a blunt probe with a wide field of view and a fine probe with very small detail resolution. This analogous to having severely limited vision with only light-dark perception over a wide field of view and the ability to see fine details only through a tiny spot in the center. Someone who must resolve many fine tactile details (like a person reading Braille) is not likely to be satisfied with a single pin sticking into a thimble on the finger he or she uses to read. To represent very fine tactile detail with a non-point field of

view requires an array of tactile pins. Tactile feedback arrays are beyond the scope of this thesis. The author has studied tactile feedback arrays, and a project to follow this thesis will add a tactile feedback array to the thimble of a PHANToM™; however, the complexity and space constraints of a tactile array preclude the in-depth analysis that will be made possible by connecting force and position sensors to a single stimulator (tactile feedback arrays have not generally used any force or position feedback to close their control loops). In addition, focusing on single point tactile feedback before broadening the investigation should provide insights that will be useful in the implementation of arrays.

4.7 Summary of Design Specifications

Table 2 summarizes the quantitative design criteria developed in this chapter. In addition to the quantitative criteria, the system requires a software driver that can be elegantly integrated into the existing force-reflecting haptic interface software.

Table 2. Summary of Quantitative Design Specifications

Gimbal mass	<90 g
Tactile feedback hardware mass	<30 g
Total mass added to system	<120 g
Orientation resolution	<2°
Roll range of motion	360°
Pitch range of motion	360°
Yaw range of motion	360°
Maximum tactor force	2 N
Steady-state force accuracy	<0.12 N

V. IMPLEMENTATION

This chapter describes the realization of the tactile feedback system in hardware and software. All results from data collection appear in Chapter VI. The chapter begins with a discussion of the two main hardware components of the system: the orientation-sensing gimbal and the tactile feedback thimble. It briefly covers the supporting electronics and the protective temperature-sensing feature. The chapter closes with a description of the PI algorithm used to control the solenoid actuator forces, and an explanation of the algorithm used to generate solenoid force commands from the virtual environment.

5.1 The Completed Hardware

5.1.1 Gimbal with Orientation Sensing. The encoderized gimbal shown in Figure 7 weighs 55.00 grams, 39% less than the 90 gram design ceiling. To help attain this low mass while maintaining low-friction performance, the supplier used the lighter Oak-Grigsby encoders, performing "surgery" to remove their substandard bearings and replace them with the smoother ones that have been used in the past with the larger encoders (the larger encoders do not come with installed bearings, which allows the designer to pick appropriate ones — the author originally faced a choice of light encoders with bad bearings or heavy encoders with good bearings). A shorter distal link was manufactured for mounting the gimbal; the shorter link weighs 16.87 grams, 2.4 grams less than the original 19.27 gram distal link. An 5.11 gram extension to the short distal link allows a quick change for use with the original thimble-gimbal when tactile feedback is not desired. The extended distal link assembly weighs 21.97 grams compared to the original 19.27 gram distal link. The addition of tactile feedback capability imposes only a 15% mass penalty on the distal link for cases where tactile feedback will not be used. This quick-change system worked quite well over a period of months with 2-3 changes per day.

5.1.2 Tactile Feedback Thimble. A detailed diagram of the tactile feedback thimble appears in Figure 8, and Figure 9 contains a photograph of the assembly. Figure 10 contains

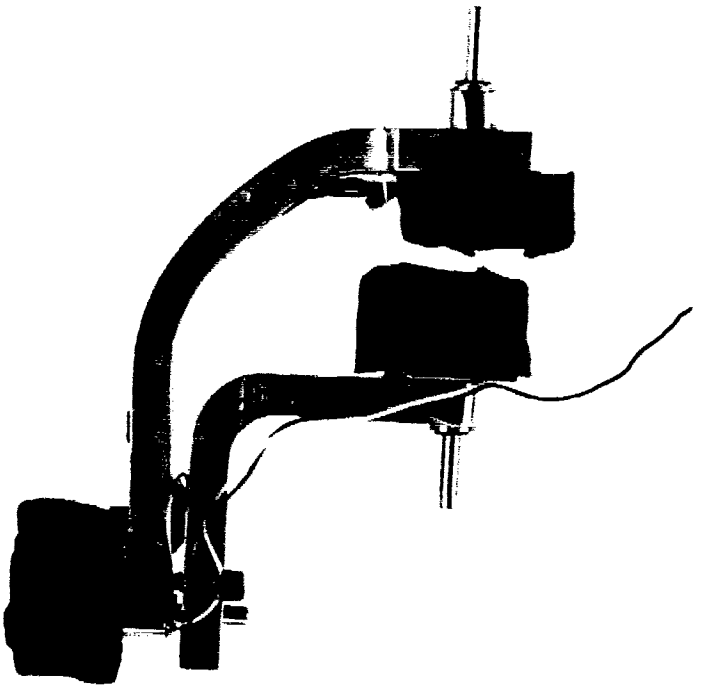

Figure 7. Encoderized PHANToM™ Gimbal

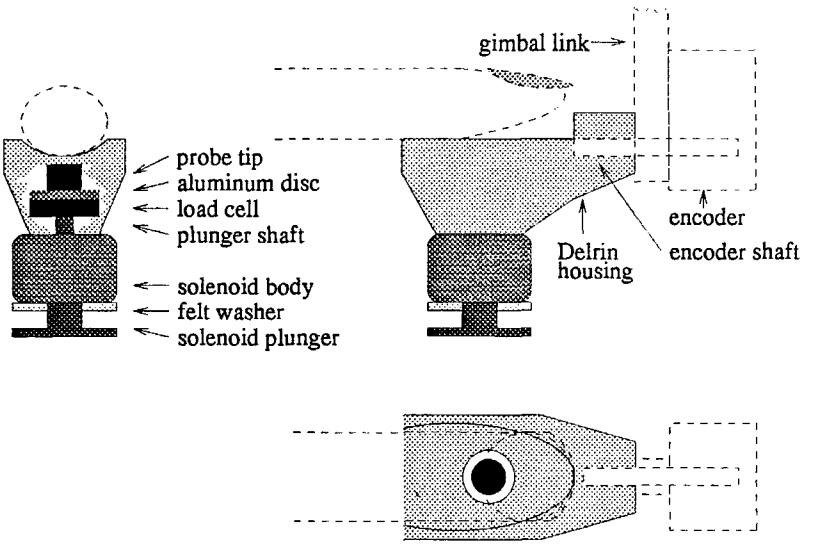

Figure 8. Drawing of Tactile Feedback Thimble

a photograph of the disassembled tactile feedback thimble. The entire assembly weighs 39.5 g, with 19.5 g for the solenoid body, 7.6 g for the moving mass, and 12.6 g for the top and bottom of the shell. (The components do not add perfectly to 39.5 g because of

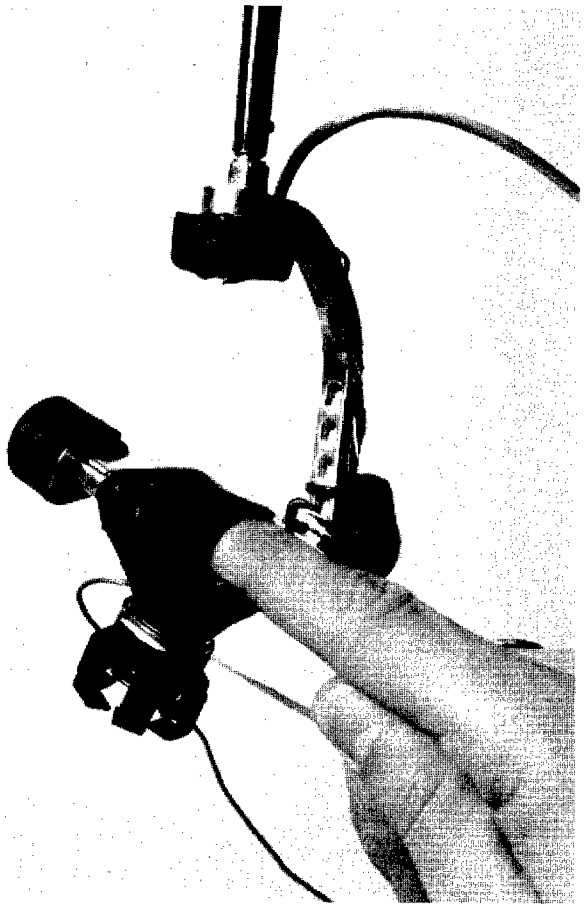

Figure 9. Photograph of Tactile Feedback Thimble

Figure 10. Photograph of Disassembled Tactile Feedback Thimble

rounding error, and the fact that cables hanging from the balance tray differently could

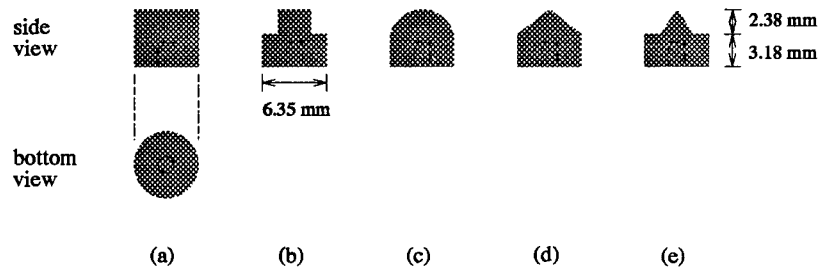

Figure 11. Tactile Probe (Tactor) Tips of Various Shapes

account for a 0.2-0.3 g difference.) Velcro™ straps secure the user's finger to the thimble. Two screws on the thimble clamp it to the distal encoder shaft.

5.1.3 Tactor Tips. The shape of the tactor tip will affect the user's perception of the device's tactile stimulation considerably. The SAI (Merkel) receptors respond to the curvature and rate of change of curvature in the skin, so tactor tips with sharper features will require much lower forces to generate a given level of perceived intensity. Because of this, sharper-featured tips should be able to generate a wider range of perceived levels of intensity with a smaller range of forces, effectively increasing the dynamic range of the device or allowing the same intensity range to be displayed with a smaller (and possibly more controllable) range of forces. Figure 11 shows the tactor tips fabricated by turning 6.35 mm (1/4 in.) Delrin rod stock and tapping the bottoms with a small hole for screwing onto the threaded post on the load cell plate.

5.1.4 Heat Sink and Spring Return Modification. After operating the tactile feedback thimble, two shortcomings became apparent. First, the solenoid reached the limits of its temperature range too fast to be useful for many applications. Second, any glitch or transient that reduced the bias force of the plunger against the finger could cause the free-floating plunger to simply fall off of the assembly. Temperature-induced drift in the load cell output often caused the plunger to fall out after a few minutes of heavy actuation.

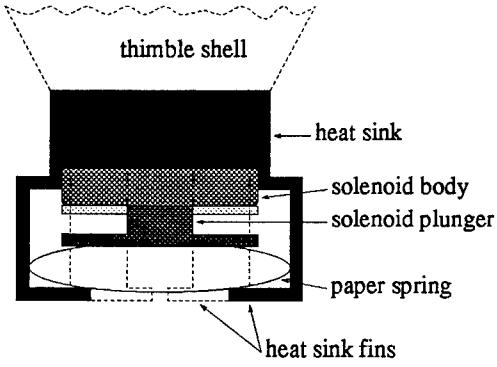

Figure 12. Heat Sink and Spring Return Mechanism Added to Solenoid

Figure 12 documents the solution to both of these problems. A light aluminum heatsink increases heat dissipation and acts as a retaining member for the solenoid plunger. An oval spring made from standard copier paper applies extremely light pressure to the solenoid, helping to keep it from dropping away from the finger and to avoid limit chatter. The heat sink improved heat dissipation so well that after ten minutes of heavy operation, the solenoid was only quite warm to the touch, rather than very hot as it had gotten without the heat sink. The heat sink adds 4.8 g to the solenoid's mass, but gives it the power capability of a much heavier solenoid.

5.2 Control System Architecture

Software running on a 100 MHz Pentium computer controls the system. A real-time interrupt-driven control loop reads sensor data and computes current commands output to the solenoid amplifier. The control loop runs at 2 KHz, and sensor electronics inside a project box filter the sensor signals with a breakpoint of about 2 kHz. The two available stain gauge channels use an Analog Devices 1B31 strain gauge amplifier chip. The LVDT channel, solenoid voltage channel (for temperature checking), and one spare A/D channel use common operational amplifiers. A Metrabyte DASH-16 A/D board makes filtered sensor data available to the control program, through its differential inputs. D/A electronics on the PHANToM™ plug-in computer card send a command signal to a Copley Controls Model

303 PWM current amplifier (identical to the three driving the PHANToM^{TM} motors). The tactile feedback solenoid connects directly to the output terminals of the current amplifier.

5.3 Solenoid Linearization

Given knowledge of the current versus force versus position response surface of the solenoid, a linearization control module could theoretically eliminate significant nonlinearities in the actuator control system. Early attempts based upon polynomial fits to a response surface determined from manufacturer's data failed to improve the controllability of the system. Further attempts using empirically-determined response surface data from the load cell and position sensor on the test stand might yield better results; however, a controller based solely upon closed-loop force control with force feedback (using gain scheduling as discussed in section 6.2) proved adequate, and further plans to characterize the response surface were discarded.

5.4 Solenoid Temperature Sensing

This application aggressively drives a solenoid and could destroy it through overheating of the coil. Consider the simple case where a constant current drives the solenoid (as it would if the solenoid were commanded to provide a constant force at a constant displacement for a long period of time). Heating of the coil causes its resistance to rise. To maintain a constant current (and thus a constant force), the controller increases the voltage, which increases the power output to the solenoid. The resultant heating of the coil further raises coil resistance, which increases power demands, etc. This situation could easily heat the solenoid to destruction if the solenoid absorbs energy faster than it dissipates it.

Under normal operating conditions, the solenoid should only be subjected to intermittent actuation. It should be able to dissipate heat fast enough to prevent overheating; however, certain circumstances such as prolonged exploration of a virtual surface may cause forces to be applied for a long period of time and lead to overheating. Aggressive driving

of the solenoid in an effort to get fast response times and high forces may also cause overheating. Appendix C presents two methods of solenoid temperature monitoring developed for this thesis. Temperature information was developed solely for the purpose of overtemperature protection, as an input to an emergency shutoff protocol, and was not used in the real-time feedback loop.

5.5 PI Control

A classic PI algorithm proved sufficient to meet the demands of this application. An algorithm from Clarke was implemented (4):

Assume the following constants,

$$K' = K_p(1 + \tfrac{h}{2T_i}), \qquad \text{and} \quad \beta = \tfrac{2T_i - h}{2T_i + h},$$

where K_p is the proportional gain and T_i is the integral feedback time constant. The control input is determined by:

$$U(z^{-1}) = K' \left\{ 1 + \frac{(1-\beta)z^{-1}}{1 - z^{-1}} \right\} E(z^{-1}), \tag{3}$$

where U represents the current input to the solenoid, and E represents the error between measured force and commanded force. The discrete equations for this control system appear below. Figure 13 shows a block diagram of the control system.

$$I[i] = K'E[i] + \Phi[i-1] \tag{4}$$

$$\Phi[i] = \beta\Phi[i-1] + (1-\beta)I[i] \tag{5}$$

I represents the current input to the solenoid, E represents the error between measured force and commanded force, Φ is the integral feedback term, and K' and β remain as defined above. Appendix E contains the source code used to implement these equations.

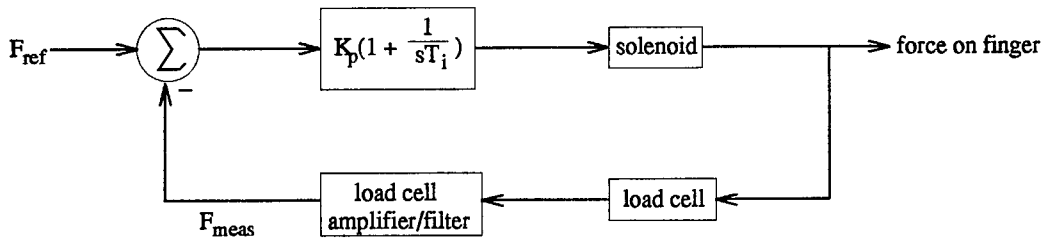

Figure 13. Control System Block Diagram

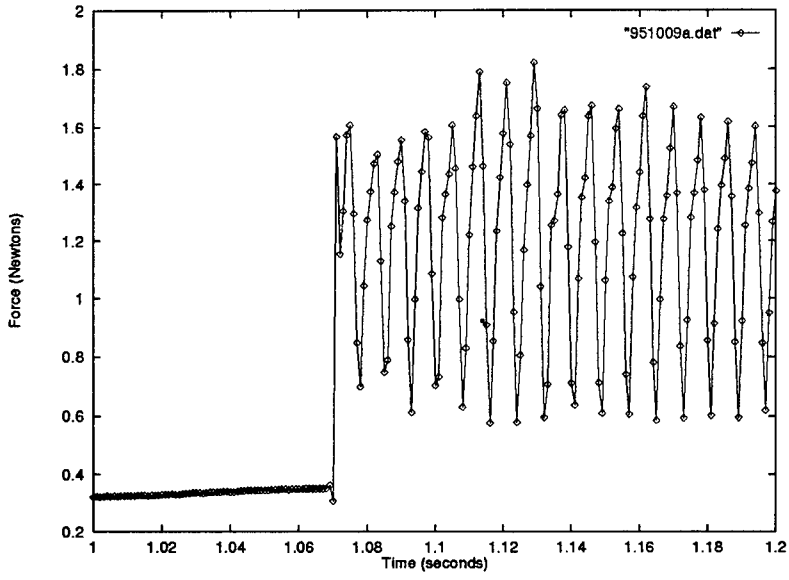

Figure 14. Oscillatory Response to a 1.5 N Step During Ziegler-Nichols Tuning

The Ziegler-Nichols' tuning rules enable the tuning of a PI or PID control system based upon the empirical performance of the system (4). A system with only proportional control is run with an increasing proportional gain until the system begins to oscillate. The gains are then set based upon the proportional gain at which the system began oscillating and the period of that oscillation. The oscillatory step response in Figure 14 was obtained with $K_p = 1.5$ and $T_i = \infty$ (no integral action). The ultimate gain $K_p = K_u = 1.5$ where the system first shows oscillation, and the period of that oscillation, ($T_u = 7.6\ ms$), facilitate the determination of the controller parameters according to the Ziegler-Nichols' tuning rules shown in Table 3. For this case, desired values of $K_p = 0.675$ and $T_u = 6.33\ ms$ emerge.

Table 3. Ziegler-Nichols' Tuning Rule (Adapted from (4))

	K	T_i	T_d
P only	$0.5K_u$	—	—
P + I	$0.45K_u$	$T_u/1.2$	—
P + I + D	$0.59K_u$	$T_u/2$	$T_u/8$

5.6 Software Calculation of Tactile Forces in a Virtual Environment

An elegant control scheme would take into account the information already available from force calculations done with the PHANToM™ and add as little extra code as possible. The following scheme was selected for implementation. The code used to drive the PHANToM™ determines desired forces along the three Cartesian axes (x, y, and z). If the user presses on a virtual surface with his or her fingerpad in the PHANToM™ thimble oriented towards the virtual surface, those forces would also exactly represent the components of the force vector that should be presented by the tactile stimulator. Likewise, if the person presses on the virtual surface with the back of his or her finger, the algorithm should be smart enough not to apply tactile stimulus to the fingerpad.

The algorithm developed defines the tactile thimble as a unit vector in space with initial value $[\ 0\ 0\ -1\ ]^T$ (finger pointed straight ahead with fingerpad downward). The kinematic code uses a gimbal-to-world rotation matrix to express the gimbal orientation vector in world coordinates compatible with the virtual model. The 3 × 3 gimbal-to-world rotation matrix is extracted from the upper left-hand corner of the 4 × 4 homogenous transform described by Craig and implemented here for the custom gimbal ((5), page 30). The next stage simply takes the cross product of the gimbal orientation vector and the world PHANToM™ force vector (the same force vector is also being fed to the PHANToM™ motors). If the fingerpad perfectly aligns with the virtual force vector, it maximizes the cross product. If orthogonal, no stimulation occurs. Nonlinear limits prevent the system from attempting reverse actuation if the cross product is negative.

The fact that the tactile stimulator can only provide the component of the world force vector orthogonal to the fingertip limits realism. For example, if the finger touches a surface with the fingerpad angled 45 degrees away from the surface, the tactile force that should be perceived as a force 45 degrees off of normal is actually experienced as a tactile force normal to the fingerpad, with magnitude 0.707 times the magnitude of the world force. Though normal forces will disappear if the finger presses the virtual surface with the fingerpad turned 90 degrees away, sideways deviations of the fingerpad at about 70-80 degrees will result in small normal forces that feel quite unnatural (one is not used to feeling even a small normal force on the fingerpad when the side of the finger presses a flat object).

To account for the tactile actuator's limitation to normal forces, an enhanced algorithm should reject tactile forces generated by force vectors far from normal to the fingerpad. This can be done either by establishing a nonlinear threshold on the cross product so that only forces closer to normal than a certain threshold are allowed to pass, or by using a continuous function like the square of the cross product that de-emphasizes forces deviating significantly from normal.

VI. RESULTS

This chapter presents an evaluation of a single-axis closed-loop force control system. Preceding chapters have presented the system requirements as defined by previous human perception research and the author's own experience. These requirements provide a context within which the quantitative performance of the control system can be assessed. A successful system will serve as a tool for future research into human perception and haptic feedback. Potential research topics include tactile signal detection, manipulative tasks, object discrimination tasks, Fitt's Law performance tasks, and more. These quantitative evaluations of human perception and performance beckon strongly, but unfortunately lie beyond the scope of this thesis. Suggestions for further work appear in Chapter VII. Some brief qualitative comments do follow the quantitative control system analysis that composes the bulk of this chapter.

6.1 Preliminary Control System Performance Measurement

6.1.1 Step Response Performance. Figure 15 shows the step response to a 1.5 N reference input with $K_p = 0.675$ and $T_i = 0.00633$. The oscillation between 1.26 and 1.36 seconds peaks at ± 0.05 N, well below the human's ± 0.12 N JND.

A closeup of the step response (Figure 16) reveals a 100% risetime of only 5 ms and a settling time of essentially zero (for settling below the human's ± 0.12 N JND). Settling to a more conservative 2% occurs in only 67 ms.

6.1.2 Steady-State Regulator Performance. Figure 17 shows that the steady-state response of the system exceeds the minimum specifications. The outer pair of horizontal lines represents the allowable range (reference plus or minus 0.12 N). The inner pair of horizontal lines indicates a more conservative 2% settling range.

6.1.3 Difficulties of the Classical Control Approach with a Nonlinear Actuator and Load. The classical control system performed reasonably well in initial tests, when tuned

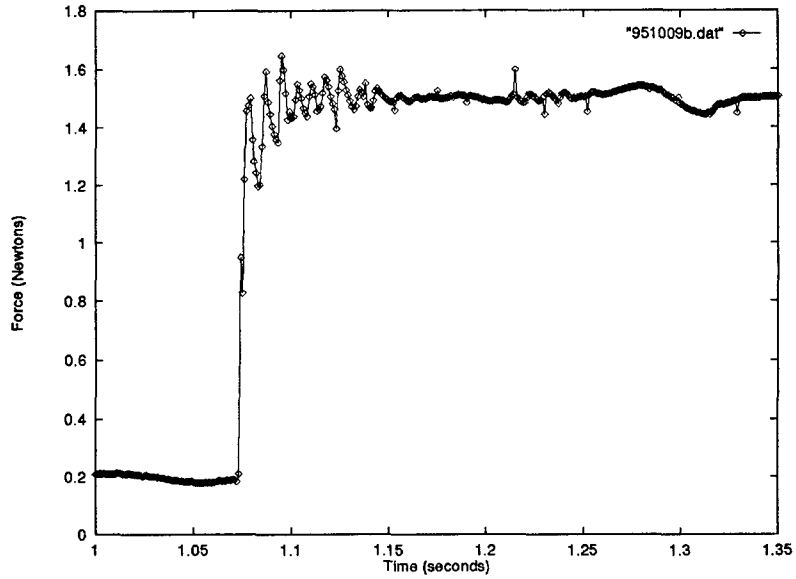

Figure 15. Step Response to a 1.5 N Input

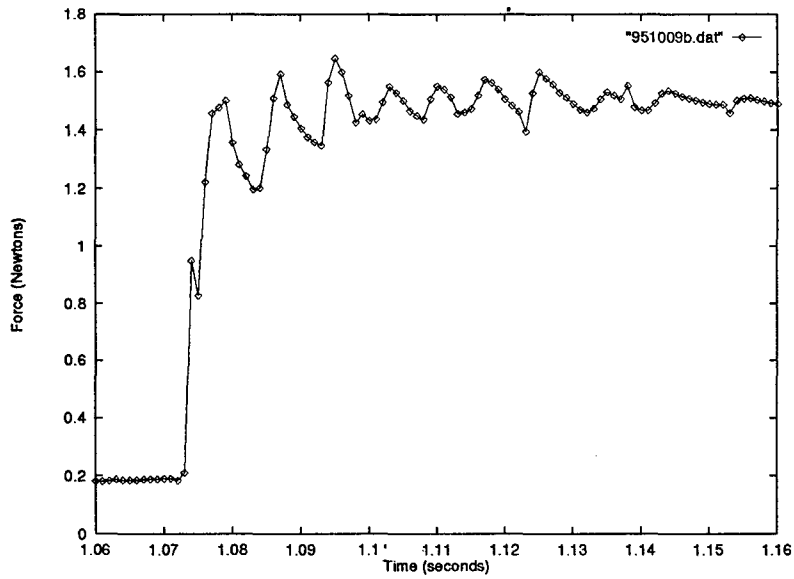

Figure 16. Step Response to a 1.5 N Input (Closeup)

for a given step size. In demonstration tests in a virtual environment, the system did not perform nearly as well. Instability and chatter destroyed fidelity in many situations when gains were set high enough to give a reasonably perceptible tactile sensation. The fact that both the actuator and the load of the fingertip have nonlinear characteristics leads

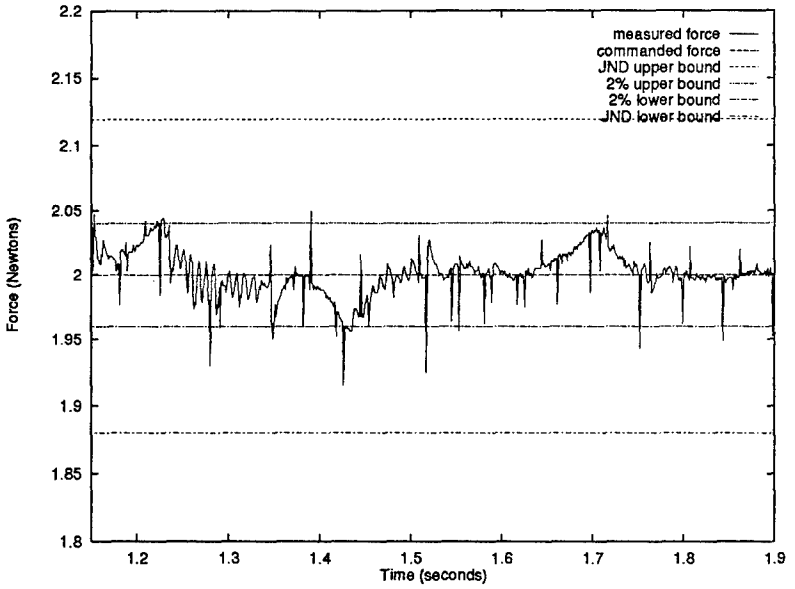

Figure 17. Steady-State Response with a 2 N Reference Force

to this problem. The closer the plunger to fully seated, the more force will be obtained for a given current. The force versus current versus position response surface is nonlinear. As the fingertip is compressed by the tactile probe, its force versus position relationship also increases nonlinearly (its nonzero second derivative indicates that the stiffness of the fingertip changes as it is compressed) (7). The fact that the load becomes stiffer just as the current-force gain of the actuator increases creates a difficult situation prone to instability.

Adaptive control comes to mind as a method for dealing with this nonlinear time-varying plant. Can a simple adaptive control technique be used, perhaps continuous gain scheduling? Gain scheduling would be practical if a predictable relationship exists between the input current and output force of the plant. This relationship could then be mathematically corrected to linearize the behavior of the system. To measure the nonlinearity of the plant, an open-loop current sine wave was input to the system, varying from 0 A to 0.55 A with a period of two seconds. The tactile probe was loaded with a human finger attempting to maintain a constant bias pressure against the probe and a surround. Figure 18 shows force versus current data plotted from ten 0-0.55 A current cycles.

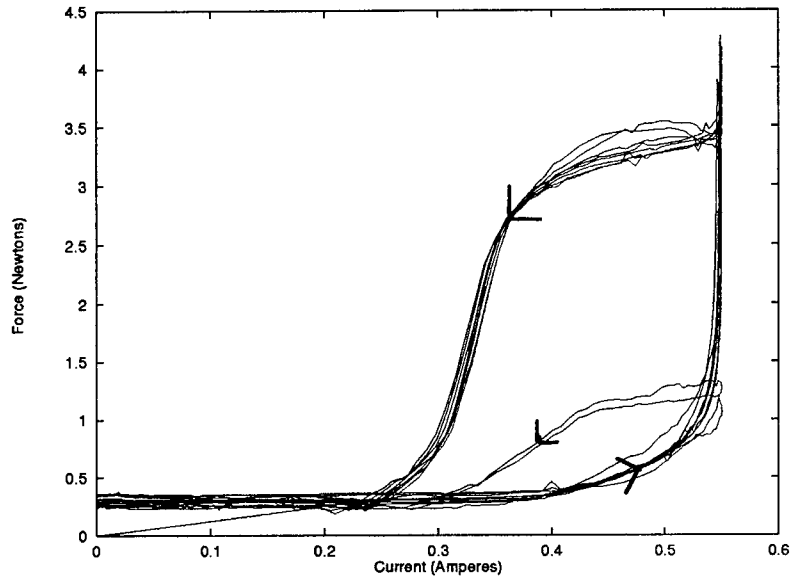

Figure 18. Cyclical Force versus Current Plot for Tactile Stimulator

Figure 18 reveals a marked and consistent hysteresis, believed to be caused by the fact that after the solenoid plunger depresses the fingerpad, it is closer to the body of the solenoid and requires much less holding current as the current is dropping. The system traces the bottom portion of the hysteresis loop shown in Figure 18 as current rises, and the top portion of the hysteresis loop as current falls. The first two cycles deviate from the others because the subject's finger did not begin with the same bias pressure that was maintained for the other eight cycles. This variable behavior with bias pressure is disturbing, since the user's bias pressure will naturally vary as he or she interacts with the virtual environment.

6.2 Continuous Gain Scheduling

Figure 19 shows results from a second trial, this time with current on the ordinate axis and force on the abscissa. With an ideal linear actuator, this plot would be a straight line with constant slope in units of Amps/Newton. In order to see how the current/force ratio changes, the slope of the plot in Figure 19 can be plotted against force. This plot, in Figure 20, contains two families of curves of the type $1/x$, and describes a gain correction factor that will be referred to as K_{iff}. The upper, tightly grouped, family represents the

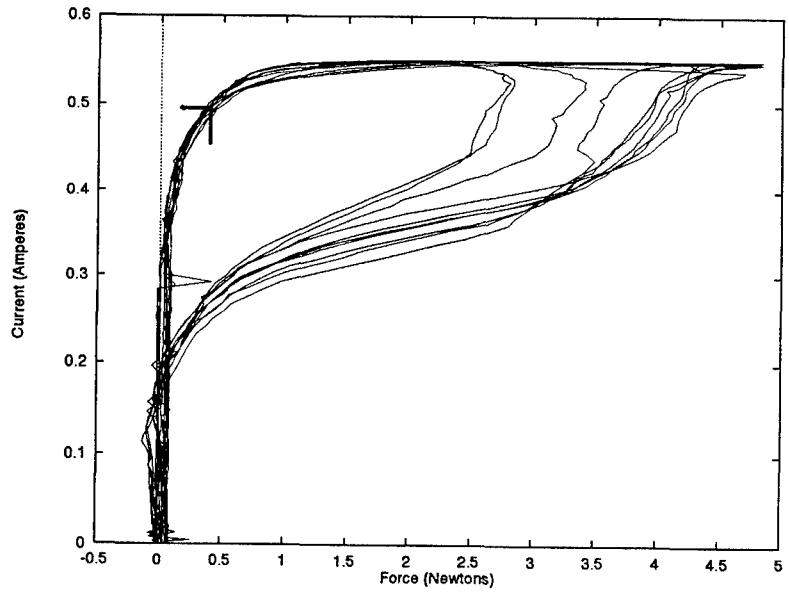

Figure 19. Cyclical Current versus Force Plot for Tactile Stimulator

slope of the tightly grouped family of curves in Figure 19 that occur as current and force rise. The lower, less tightly grouped, family represents the slope of the less tightly grouped family of curves in Figure 19 that occur as current and force fall. The dotted line in between the two curve families represents the gain correction approximation:

$$K_{iff} = \frac{0.4}{F_{meas}} \tag{6}$$

where F_{meas} is the measured force at the tactile probe.

Continuous gain scheduling was implemented by applying the K_{iff} correction term to the error term. Equation 3 is modified to include the correction term:

$$U(z^{-1}) = K' K_{iff} \left\{ 1 + \frac{(1-\beta)z^{-1}}{1-z^{-1}} \right\} E(z^{-1}), \tag{7}$$

This results in the following replacement for Equation 4:

$$I[i] = K' K_{iff} E[i] + \Phi[i-1] \tag{8}$$

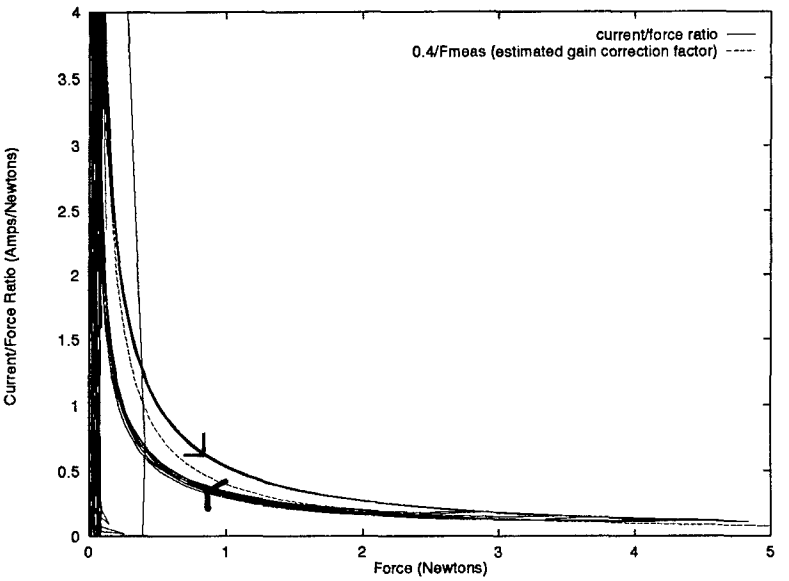

Figure 20. Current/Force Ratio as it Varies with Force

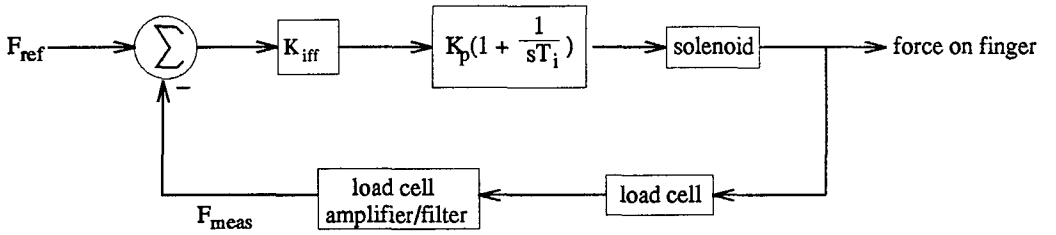

Figure 21. Control System Block Diagram with Gain Scheduling

The integral feedback term Φ, defined in Equation 5, becomes an integral of the corrected error. The continuous gain scheduling algorithm described in this section effectively eliminated instability problems in the system. A revised control system block diagram appears in Figure 21.

6.3 Final Force Control Results for System with Gain Scheduling

6.3.1 Step Response. Figure 22 shows a step response to the maximum allowable force of 2 N obtained using the adaptive algorithm. It exhibits a marked 50% overshoot, but the task requirements can accommodate such an overshoot. Step changes in tactile force

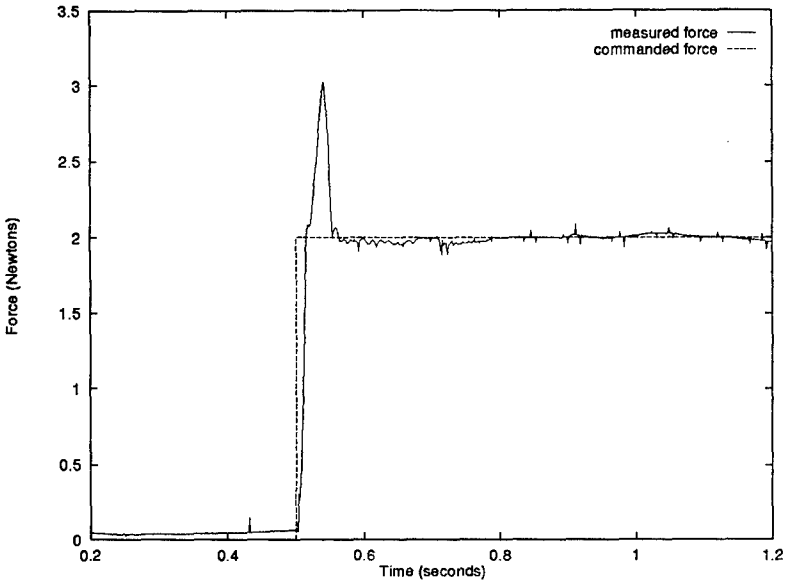

Figure 22. Step Response of Tuned Solenoid Tactile Feedback System

typically occur when the finger touches an object, and a force spike is a typical event as the finger decelerates. A less-aggressive tuning of the system or the addition of derivative action to the PI controller could used to reduce the overshoot by increasing the damping. It takes the system about 15 ms to go from 0 N to 2 N, and about 11 ms to go from 0.2 N to 1.8 N.

6.3.2 Sine Wave Tracking. Figures 23 through 26 show tracking behavior for the system following 0.5 N $\pm$ 0.2 N sine waves at frequencies between 2 Hz and 100 Hz. The same data used for these plots were also used to generate the magnitude and phase response plots in section 6.3.3. All data were taken with the servo loop running at a sampling rate of 2 kHz. The data for the 2 Hz sine wave in Figure 23 were decimated to 100 Hz, and the data for Figures 24 through 26 were decimated to 1 kHz.

The nearly perfect tracking performance in Figure 23 suffers only slightly from hysteresis-induced error as it returns from the high and low extremes of the sine wave. Performance at 10 Hz (Figure 24) is still admirable, though significant hysteresis-induced tracking error begins to appear, as does phase lag (see Figure 28 for a plot of phase lag versus frequency).

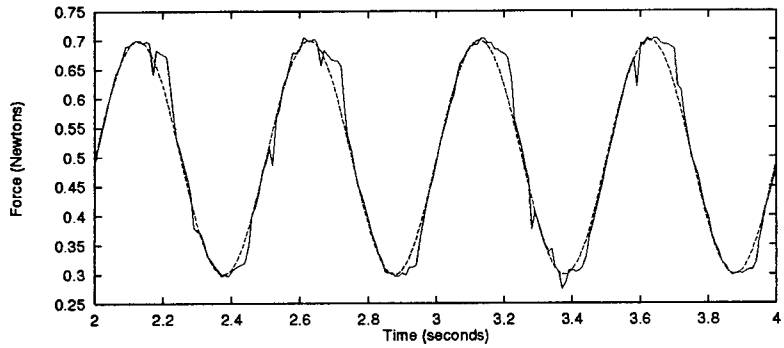

Figure 23. Tracking Response for a 2 Hz Sine Wave

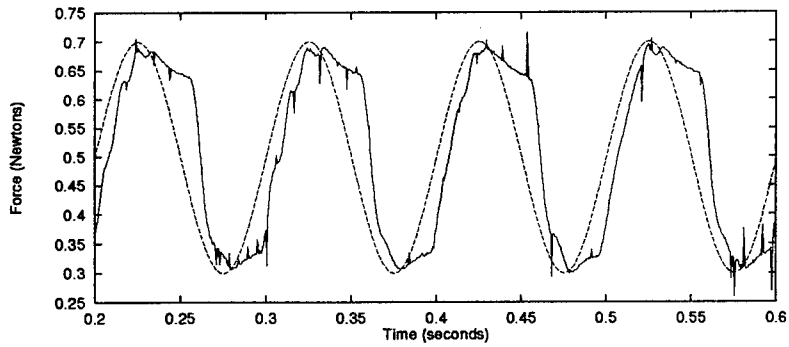

Figure 24. Tracking Response for a 10 Hz Sine Wave

Hysteresis-induced error (error not simply attributable to phase lag) does not seem to get any worse at 40 Hz (Figure 25), but phase lag continues to increase to nearly 180 degrees at 100 Hz (Figure 26).

All tracking plots reveal a noticeable amount of noise, though this noise did not seem to be perceptible by the finger of an observer using the device (which was not unexpected, given the human's pressure perception limits). Noise reduction might be attempted by significantly lowering the cutoff of the load cell filter from 2 kHz to 400 Hz. Figure 26 shows noise at 200 Hz (at the peak and trough of every sine wave). This noise is most likely aliased down from 20 kHz spikes generated by the PWM current amplifier that slip by the capacitors in the load cell filter. Adding ceramic capacitors to the filter may help to trap these high-frequency spikes.

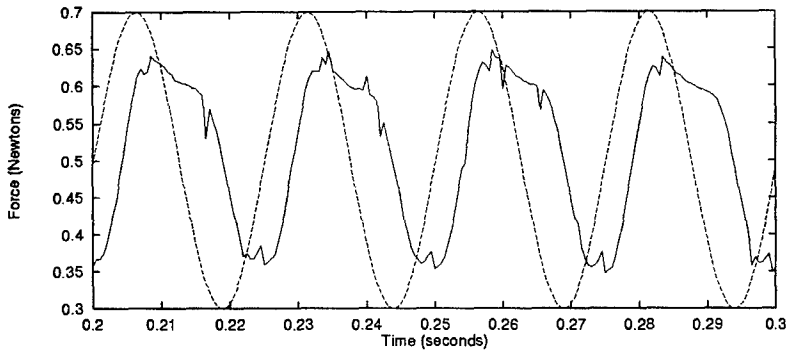

Figure 25. Tracking Response for a 40 Hz Sine Wave

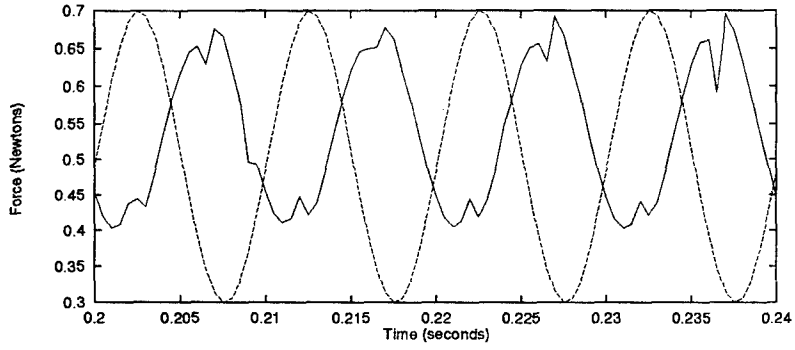

Figure 26. Tracking Response for a 100 Hz Sine Wave

6.3.3 Frequency Response. Figure 27 shows the frequency response of the solenoid tactile feedback system when loaded with a finger in the thimble. It documents the performance of this nonlinear system with the particular operating conditions and adaptive gain scheduling described above. It shows a full response out to 160 Hz that is nearly level to 40 Hz. The response falls at a rate of 380 dB per decade between 160 Hz and 200 Hz. Sine waves of the form 0.5 N $\pm 0.2 sin(2\pi samplenum)/(2000 * T)$ N drove the system. Data for the solid-line plot came from peak-to-peak measurements of the output, and data for the dashed-line plot came from negative amplitude measurements only (how far force dropped from 0.5 N toward the goal of 0.3 N.)

The negative-amplitude-only and the full peak-to-peak plots represent different aspects of the system. Unlike a conventional voice coil or electric motor, solenoids can only

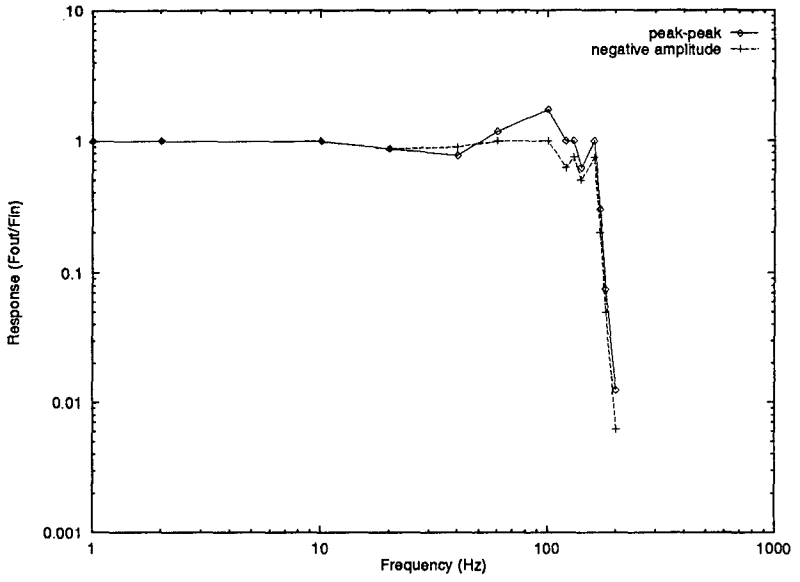

Figure 27. Frequency Response of Loaded Solenoid Tactile Feedback System (Magnitude Plot)

exert force in one direction. The negative-amplitude-only plot measures the ability of the system to rapidly let forces against the finger drop. Since it cannot apply energy to force the plunger away from the finger, the negative-amplitude-only plot will decrease more quickly with increasing frequency, but will also be less prone to instability or other wild behavior. Notice the lack of a resonance in the negative-amplitude-only plot.

Figure 28 shows the phase response of the loaded solenoid tactile feedback system. The solid line on the plot with the key notation "rise (actuated)" indicates the phase lag in the leading slope of the force sine wave, as the solenoid plunger drives the tactor tip into the finger. The dotted line on the plot with the key notation "fall (rebound)" indicates the phase lag in the trailing slope of the force sine wave, as current to the solenoid plunger drops and the tactor tip rebounds from the fingerpad. Since this retreat from the finger is not aided by the actuator, the rebound phase lag can be expected to be greater than the actuated phase lag, as Figure 28 illustrates. This discrepancy in the phase plots for active and rebound stages occurs for the same reasons that the two plots in Figure 27 differ.

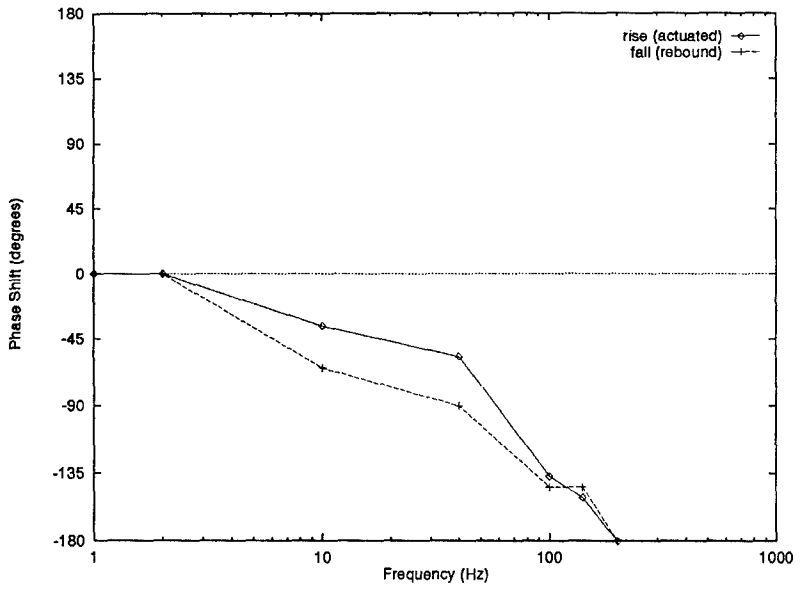

Figure 28. Frequency Response of Loaded Solenoid Tactile Feedback System (Phase Plot)

6.3.4 Steady-State Accuracy. Figure 29 shows a steady-state response to a step input. Two pairs of tolerance lines on the plot indicate that the steady-state performance stays within two sets of limits. The inner pair of tolerance lines represents the 2% settling limit commonly used with control systems. The system drops within this limit 62 ms after the step input, immediately after the end of the overshoot spike. The outer pair of tolerance lines represents the steady-state force variability perception threshold estimated in section 4.5. Clearly the system satisfies the accuracy requirement motivated by the human JND for pressure perception. The peak steady-state tracking error of about 0.03 N for this system also compares favorably to the mean steady-state tracking error of a human finger measured by Srinivasan and Chen to be 0.04 N (35).

6.3.5 Dynamic Range. The ratio of the highest usable signal to the lowest usable signal determines the dynamic range of the system. This ratio changes with frequency because neither the highest usable signal or the lowest usable signal remain constant over the frequency spectrum. The actuator and frequency response of the control system cause the highest usable force to change with frequency. The human's sensory capabilities cause

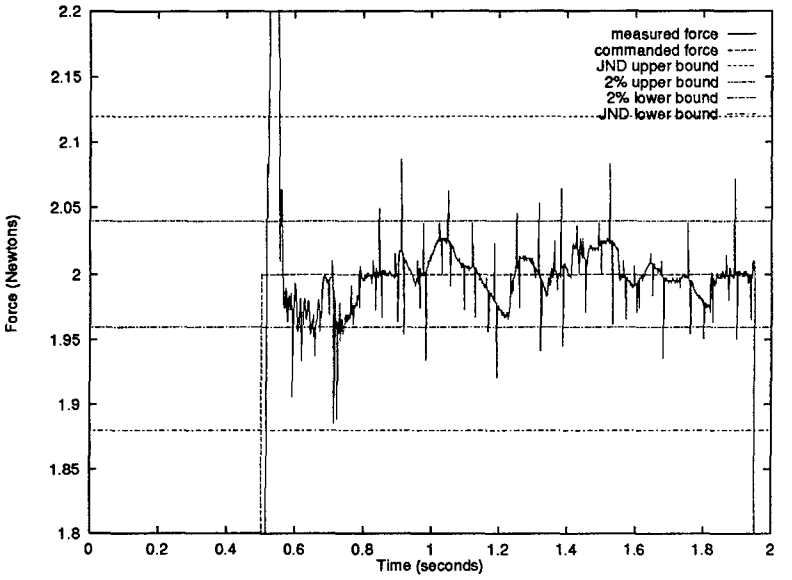

Figure 29. Settling Behavior of Tuned Solenoid Tactile Feedback System

the lowest usable signal to change with frequency. The maximum 2 N signal at steady-state remains steady past 10 Hz and then drops off after 160 Hz. (The resonance in the Bode plot between 50 and 120 Hz technically increases the maximum force, and thus the dynamic range, but this is not a desirable effect.)

Determination of this system's minimum usable force as it varies with frequency would require rigorous threshold testing with many trials and a number of subjects. Anecdotal evidence and extrapolations from earlier published data will contribute to a working hypothesis here which should be interpreted with caution. The steady-state case with only step changes in force is similar to the experiments by Tan cited in section 4.5 during the discussion of human pressure perception. Extrapolation from Tan's conclusions indicated a minimum appreciable force change of 0.12-0.18 N. Selecting 0.18 N for the most conservative dynamic range estimate and comparing to the maximum steady-state force of 2 N gives a dynamic range estimate of 21 dB.

With just the slightest bit of frequency content, the dynamic range increases drastically, since the minimum appreciable change (JND) falls from 0.18 N to 0.01 N (anecdotal

data). This translates to a dynamic range of 46 dB at 2 Hz. At 10 Hz, the JND has dropped even more; one user perceived sinusoidal force variations at 0.0075 N, slightly elevating the dynamic range to 48 dB. As frequency increases, the perception threshold for sinusoidal force variations may drop, but the maximum attainable force at that frequency will also drop as the response of the actuator rolls off.

At 200 Hz, assuming that the system has been adequately linearized (a dubious assumption), a 2 N commanded sinusoid will produce a 0.025 N sinusoidal output due to the low gain at this frequency. The minimum perceptible force sinusoid for one subject was 0.007 N peak-to-peak, leading to an estimated dynamic range of 11 dB. As the system bandwidth continues to fall, and the human vibration perception threshold rises past 250 Hz (see Sherrick and Cholewiak (32)), the dynamic range will continue to fall.

6.3.6 Signal-to-Noise Ratio. Qualitatively, noise did not have a substantive effect on the performance of the final system. Assuming relatively consistent noise, a quantitative value for the signal-to-noise ratio obviously depends on the signal strength. Since forces perceptible with this system range from a few hundredths or thousandths of a Newton (0.05 N vibrations at 200 Hz were perceptible, and 0.007 N vibrations seemed to be perceptible in at least one trial) to 2 N, the signal-to-noise ratio will vary widely.

For a nominal signal-to-noise ratio estimate, data from 12 trials with a reference signal 0.5 N $\pm 0.2 sin(2\pi * samplenum)/1000$ at 2 Hz were taken from the loaded system. Use of a 2 Hz signal, with nearly perfect tracking and zero phase lag, assured that differences between measured force and the reference signal were attributable to noise and not artifacts in the control algorithm. The data yielded a mean signal-to-noise ratio of 61 dB with a standard deviation of about 2 dB.

Data from twelve trials with a very small reference signal generated a worst-case estimate of signal-to-noise ratio. The trials used a reference signal 0.5 N $\pm 0.05 sin(2\pi * samplenum)/20$ at 2 Hz. The signal strength estimate considered only the AC component of the signal (± 0.05 N), neglecting the large DC offset to concentrate on the small information-

carrying component of the signal. The trials resulted in a mean signal-to-noise ratio of 18.8 dB with a standard deviation of 1.1 dB. Anecdotal reports by one human subject indicate that he could easily perceive this signal, though it did not appear to be very far above threshold.

One difficulty with the time-domain measurement of signal-to-noise ratio here is that it includes electrical noise at frequencies too high to possibly effect the forces of the tactile probe. A frequency-domain method that neglected frequencies past the bandwidth of the tactile feedback system would produce more relevant, and probably higher estimates of signal-to-noise ratios. Better filtering (perhaps adding ceramic capacitors to the existing filter) would reduce electrical noise, and might as a result reduce any mechanical noise that might originate as electrical noise and be aliased down to lower frequencies.

6.4 Comments on the Subjective Percept

This section contains an anecdotal description of early experience with the tactile feedback system. Human perception and task performance experiments suggested in section 7.6 should be pursued to obtain quantitative results. When compared to the PHANToM™ without tactile feedback, the present system afforded the user an enhanced perception of fingertip contact with an object. Actually feeling pressure on the fingerpad, rather than a more generalized feeling of finger force available with a non-tactile thimble, felt more "real." Tapping a surface resulted in a convincing tactile force impulse on the fingertip, and running a finger along a smooth surface allowed a seemingly fine sense of the normal force against the surface.

The most obvious drawback was the mass added to the fingertip. It caused a noticeable reduction in the crispness of the PHANToM™'s vibratory response to a textured surface, though the reduction was mitigated by the fact that high-frequency vibrations could be felt through tactile feedback at the fingertip where they could not be felt before. Inertia was experienced not just as Cartesian inertia, but as rotational inertia as well.

With the 18 gram nylon-reinforced Delrin gimbal and thimble originally supplied with the PHANToM™ rotational inertia is imperceptible. The custom gimbal fabricated for this effort not only weighs more, but has larger radial dimensions which increase its apparent inertia about the pitch and yaw axes. The mass of the solenoid and tactile thimble add significant rotational inertia about the roll axis.

With the adaptive gain scheduling modification, the control system behaved well, though it has not been tested with a wide variety of users. Additional adaptive improvements might be necessary before the device would be acceptable to a novice user with unknown finger characteristics. Of the two major areas for potential improvement, mass reduction and control system upgrades, mass reduction should take the highest priority. Though immediate opportunities for continuous improvement exist, the system in its present state offers significant capabilities for human factors analysis.

6.5 Summary of Results

Table 4 shows the actual performance of the system compared to the quantitative design criteria established in Chapter IV. In addition to the attainment of the quantitative specifications, the software driver described in section 5.6 meets the criteria for an elegant interface to the existing force-reflecting virtual environment algorithm. Note that the yaw range of motion for the gimbal falls slightly short of the desirable range of motion. This occurs because the top of the solenoid collides with the gimbal within a small section of the roll range of motion. This does not have a significant effect on performance, since even with full arm, wrist, and shoulder movement, it is difficult for subjects to reach the point where the solenoid collides with the thimble.

Table 4. Summary of Quantitative Results

Feature	Design Specification	Actual Specification
Gimbal mass	<90 g	55 g
Tactile feedback hardware mass	<30 g	39.5 g
Total mass added to system	<120 g	94.5 g
Orientation resolution	<2°	0.7°
Roll range of motion	360°	350°
Pitch range of motion	360°	360°
Yaw range of motion	360°	360°
Maximum tactor force	2 N	>2 N
Steady-state force accuracy	<0.12 N	<0.03 N

VII. DISCUSSION AND CONCLUSIONS

The completion and characterization of the tactile feedback system described in this thesis marks a beginning, rather than an end, to this program of work. Further work should include improvements in system performance and utilization of the system for its intended purpose — research of haptic perception issues. This chapter offers suggestions for improvement to the current system in two areas: mass reduction and control system upgrades. Suggestions for alternative approaches to the problem of tactile feedback on a force-reflecting platform appear next. The chapter closes by offering some potential topics for future research.

7.1 Mass Reduction

Since the additional mass of the tactile feedback system has emerged as perhaps the greatest performance limiting factor, this section will consider ways to reduce the mass. How much can redesign reduce mass while conforming to the current paradigm of an orientation-sensing gimbal with a tactile force actuator? (Section 7.5 considers whether paradigm shifts exist that might cast off some of the disadvantages of this approach while maintaining many of the advantages.) Table 5 lists masses of all system components and subcomponents, along with their percentages of the total mass. Components responsible for a high percentage of the total mass should receive first consideration for mass reduction.

The tactile thimble-gimbal assembly weighs a total of 94.5 g, but since the original thimble weighs about 18 g and the shortened distal link weighs about 2 g less than the original one, the additional mass of the tactile system amounts to only 74.5 g. Each major subcomponent, the orientation-sensing gimbal and the tactile feedback thimble, accounts for a large portion of the total mass. The gimbal accounts for the largest portion (58.2%), and may be the best target for mass reduction.

The gimbal encoders account for over a third (36.5%) of the total system mass. In addition to their large mass percentage, two of the three sit far from the center of the

Table 5. Masses of System Components

Description	Mass (grams)	Percentage of total
Orientation-sensing gimbal	**55.0**	**58.2**
Three encoders (Oak-Grigsby)	34.5	36.5
Gimbal links, bearings, etc.	20.5	21.7
Tactile feedback thimble	**39.5**	**41.8**
Moving mass	7.55	8.00
solenoid plunger (5.35 g)		
load cell and plate (2.38 g)		
Delrin tactor tip (0.18 g)		
Solenoid body	19.5	20.6
Delrin shell (& 6 screws)	12.6	13.3
TOTAL	**94.5**	**100**

thimble and apply large rotational as well as translational inertias to the fingertip. Technical Research Associates (Salt Lake City, UT) has developed small rotation sensors (not yet commercially available) that would probably weigh four grams or less. Sarcos Research Corp (Salt Lake City, UT) may also soon produce lightweight rotation sensors. Commercially-available Hall-effect sensors might be suitable if they are not affected by the solenoid's magnetic field. Use of such rotation sensors would reduce the total mass by about 22.5 g (24%). The current gimbal link design leaves very little room for mass reduction, but perhaps 3 g of the 20.5 g mass could be shaved off with more cavities or different material selection, representing a 3.2% reduction in the total mass.

The tactile feedback thimble, with less of the total mass than the gimbal, and half of its mass committed to the off-the-shelf solenoid, offers less opportunity for mass reduction with the current paradigm. Perhaps 2 g could be shaved off of the Delrin shell for another 2.1% reduction in total mass. Another 1 g can be eliminated from the plunger by replacing its stainless steel shaft with a Delrin shaft (without affecting performance). The mass reductions proposed for the rotation sensors, gimbal links, thimble shell, and plunger total 28.5 g, a 30% savings that would result in a total system mass of 66 g. This 66 g mass means about 46 g added on to the original equipment mass (compared to the 74.5 g added

on by the current tactile hardware). The improvements noted above would reduce the mass attributable to the addition of tactile feedback by 38%. Based upon this author's experience, such a savings would improve performance markedly, but the current approach would still have enough drawbacks to motivate investigation of other paradigms.

7.2 Control Algorithm Improvements

Efforts to improve the control algorithm might have beneficial effects in at least two ways. First, the system does not use the available bandwidth of the human tactile sense. Its response has degraded -40dB by the time it reaches 200 Hz, and the human Pacinian receptors reach their point of highest sensitivity at 250 Hz. Useful information can be presented up to a few hundred hertz beyond that figure. The above-mentioned 1 g reduction in moving mass (obtained by used a Delrin plunger shaft) can be expected to offer some improvement in bandwidth. Another way to increase the bandwidth of the system might be to increase the range of stable gains available. An improved adaptive control scheme aimed at reducing the lingering effects of nonlinearity in the current-force gain might allow faster control system roots. An improved adaptive approach might also help in a second way by making the system more robust to differing bias pressures from user's fingers or to shifts of finger position within the tactile thimble. This would mean that feedback gains would no longer have to be conservatively tuned for the worst-case scenario, and the system would also be more robust to the finger characteristics of different users.

If one were willing to try position feedback rather than force feedback, a photoemitter/detector pair could be affixed to the side of the solenoid body, with a reflector riding in an "outrigger" fashion on the side of the plunger. This would eliminate the mass of the load cell, which comprises 32% of the total moving mass, offering a significant chance for bandwidth improvement.. Virtual forces could be mapped to a desired tactor position using finger models such as that of Gulati (7).

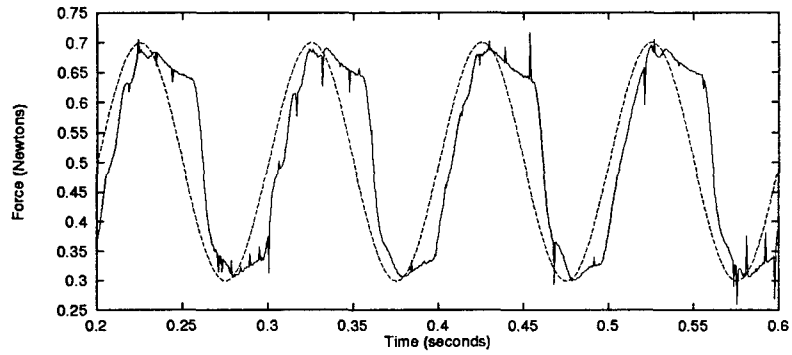

Figure 30. Tracking a 10 Hz Sine Wave with Curve-Fitted Feedback Linearization

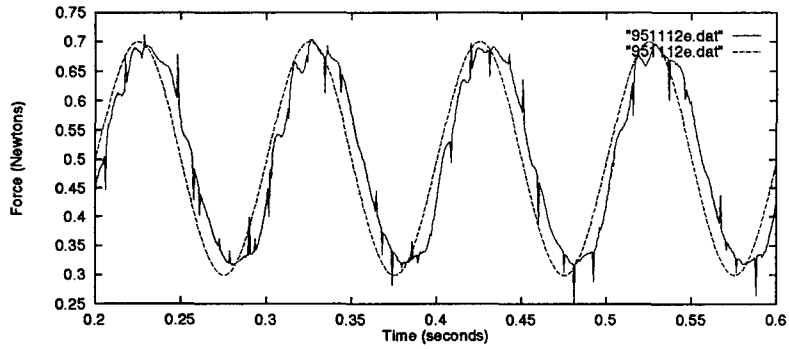

Figure 31. Tracking a 10 Hz Sine Wave with Sensor-Based Feedback Linearization

7.2.1 Sensor-Based Feedback Linearization. The results presented in Chapter VI were obtained from a system with feedback linearization based upon a fixed equation estimating the current/force ratio as it varies with force. This equation was obtained by fitting a curve to a plot of empirical data from a certain set of operating conditions (see Figure 20 on page 44). This curve does not fit the empirical data perfectly (particularly because of hysteresis in the system), and operating conditions may vary widely. An approach that linearizes feedback based upon a knowledge of the actual current/force ratio measured in real time might avoid the problem of imperfect curve fit and perform well under unpredictable operating conditions.

Such an approach was tested using a twenty-sample moving average of the commanded current, I_{sol}, divided by the measured force, F_{meas}. A comparison of curve-fitted lineariza-

tion performance in Figure 30 to sensor-based linearization in Figure 31 shows a significant improvement in linearity and a slight improvement in phase lag that make further investigation of this technique appealing. The system was successfully demonstrated to a group of 10-15 people using the sensor-based linearization algorithm, proving that it is robust enough to handle a group of novice users with a variety of finger shapes and sizes.

7.3 Sensor Robustness

Another refinement will make the system more usable over extended periods and under variable conditions. A problem exists with the load cell; over a period of a few minutes of operation, the load cell output drifts upward. This first becomes apparent to the operator as a reduction in the bias force of the tactile probe (the actual force is lower than the system thinks it is). The bias force eventually disappears and continued drift effects system stability since the gain scheduling depends on an accurate knowledge of force.

Heat from the solenoid body causes the temperature of the solenoid plunger and shaft to rise. The shaft inserts into the center of the load cell (Figure 8 on page 31), transferring heat to it by conduction. Ordinarily the full-bridge load cell used in the tactile feedback thimble would be temperature-compensated up to 71 C (160 F), but the heat conducted into the inner diameter of the donut load cell appears to create a temperature gradient across the load cell, heating the bridge members unevenly. Insulating the load cell from conducted heat or heating it uniformly to 71 C (160 F) would solve the problem. Insulation seems most practical for this application. The 3.175 mm (0.125 in.) solenoid shaft could be mated with a 2.54 mm (0.10 in.) shaft made of a material with low thermal conductivity. Ambient heat would not be as much of a concern, since the Delrin shell shields the load cell from the solenoid body; conduction through the steel shaft is currently the main method of heat transfer. Convection heating would also occur more slowly and would likely not exceed the compensation capabilities of the load cell (the manufacture tests the load cells for temperature stability in a convection oven).

Shortly before completion of this work, a modified plunger was tested. The modified plunger has a stainless steel shaft that was cut near its midpoint and mated to a Delrin shaft for connection to the load cell. This modification effectively eliminated the heat conduction problem. It also reduced the mass of the 5.35 g plunger by 0.55 g (this represents a 7% reduction in the 7.55 g moving mass). Since the non-ferrous stainless steel shaft does not contribute to the solenoid's generation of forces, completely replacing it with a Delrin shaft should not affect performance. Complete replacement would have the additional advantage of reducing the moving mass by at least 1 g.

7.4 Psychophysical Concerns

The present device does not differ from generation after generation of tactile stimulation hardware, in that it provides feedback only of forces and vibrations normal to the surface of the fingerpad. If this sort of feedback were sufficient we could go satisfy all our needs for haptic information in "real life" by repeatedly picking our hands up and placing them down on objects, never allowing the objects to have sliding contact with our skin. The current device obviously presents a subset of the stimuli available to our fingertips under normal circumstances. Some contemplation of the boundaries of that subset should shed light upon its potential utility.

The **Meissner corpuscles (FAI)** detect localized slip and surface features too small to activate the SAI's. Both capabilities are thought to be related to the movement of the papillary ridges. The FAI afferents probably do not play the most significant role in the perception of the present tactile stimulator, except perhaps as contributors to texture perception when excited by 20-50 Hz vibrations. **Merkel disks (SAI)** are sensitive to compressive stress (curvature). They probably receive significant stimulation from the various-shaped tactile probe tips of the current system, though the fact that the stimulus acts normally, with no tangential motion, may reduce the magnitude of the SAI activity. **Pacinian corpuscles (FAII)** respond in a poorly-localized fashion to high frequency information. This helps in detecting unanticipated contacts and in switching from position to

force control mode, for example (20). **Ruffini endings (SAII)** are sensitive to lateral skin stretch, of which little happens with the present device. In summary, the present device seems most likely to excite SAI afferents, with stimulation of FAI and FAII afferents under some circumstances.

7.5 Alternative Tactile Feedback Approaches

Two alternative enhanced feedback methods involve vibration feedback (a vibrating actuator to reproduce vibratory events from the remote or virtual environment). The first method would use cutaneous tactile feedback to a specific site(s) on the fingerpad. Piezoelectric actuators weighing only a few grams might replace the bulky 20 g solenoid, but their restriction to a single resonant frequency would severely curtail the information content and perceived reality of the tactile signal. Miniature voice coil actuators of the type used in headphones would have a larger bandwidth and still be likely to weigh much less than the solenoid. A voice coil actuator would also have a useful linear range and would avoid the necessity of a load cell if driven open-loop.

The second method presents vibration information to the entire fingertip at no specific cutaneous location, as reported by Howe's laboratory (Kontarinis and Wellman)(18, 37). This method works well to almost seamlessly extend the perceived bandwidth of the haptic interface.

Should tactile cues be presented to the whole fingertip or a specific location on the skin? Skin contact location can give vital cues for manipulation, but the addition of specific site stimulation will likely have benefits over generalized stimulation only if the site stimulated correctly corresponds to a point of contact in the virtual or remote environment. Making the correct correspondence requires extra hardware such as encoders to sense orientation, and more stimulators if more than one site will be stimulated. The appeal of using only general vibration information is that the mass of orientation-sensing encoders can be avoided.

Applying a miniature voice coil actuator to one site on the fingerpad would preclude the use of Howe's technique to excite the entire fingertip unless a second voice coil were used (or the coil could be brought into and out of contact with the finger – which might still require a second actuator). An actuator that could both vibrate away from the fingertip and could exert a DC displacement to touch the fingertip and vibrate might also serve a dual function. A spring-loaded solenoid or voice coil might be able to do this.

The strengths of various methods might be combined in a hybrid approach that uses a small voice coil actuator for whole-fingertip wide-bandwidth vibration feedback and four tiny piezoelectric actuators for specific site stimulation on the fingerpad, tip, and sides. It would certainly be interesting to see how a user would experience wide-bandwidth whole-fingertip vibration with low-amplitude single-frequency stimulation at a particular site. Would the richness of the wide-bandwidth signal work in concert with the specific site cue? Would the single-frequency stimulation of the piezoelectric crystals impede perception of the wide-bandwidth voice coil signal? Since the major mass components of the current system are the encoders and the solenoid, the hybrid approach suggested above with lightweight encoders and a voice coil actuator weighing about 10 g offers the best promise of capability combined with low mass.

7.6 Future Work

The current system has been developed as a tool for research into haptic perception of, and performance in, synthetic and remote environments. Research that elicits information on the sensory information that aids human performance in haptic tasks contributes both to an understanding of the human haptic sense and to knowledge of how to design elegant systems that provide adequate "presence" to the user.

Future research using this device could follow many avenues. The most valuable approach may be to explore its differences with other systems. Howe, Kontarinis, and Wellman have already shown the effectiveness of a generalized finger vibration feedback

device (16, 18, 37). The present device differs in two major ways: it applies a stimulus directly to a specific point on the fingerpad, and it can sustain steady-state forces against the fingerpad in addition to being able to vibrate. One interesting experiment to compare the two systems could test to see whether a tactile actuator in contact with a specific spot on the skin would be more effective at eliciting the adaptive motor responses that Johansson observed in response to local slip events (13).

Other research might explore implementation alternatives using the current device. For example, for what tasks is a blunt fingertip and sharp tactile probe more useful than a virtual point fingertip and point tactile probe? Exactly how sharply focused should the tactile probe's region of sensitivity be (how big of an area on the virtual finger should activate the tactile feedback stimulator)?

The present stimulator can excite the Pacinian system, which according to Lederman and Pawluk helps to detect unanticipated contacts (20). This detection of a state transition may inform the operator's muscle control state (e.g. instigate a switch from position to force control). An experiment might be conducted to confirm that localized stimulation does not aid in the performance of tasks with unanticipated contacts when compared to non-localized Pacinian stimulation like that provided by Kontarinis and Howe (18).

Since texture discrimination seems to have a significant intensive component (as opposed to the spatial component which cannot be presented well with a single-element stimulus), an experiment could compare texture discrimination capability with the present system, a non-tactile PHANToM™ and Howe's generalized vibration device. To maintain the same force-reflection dynamics, the current system might be placed on Howe's force-reflecting finger master (9). Texture discrimination experiments could be run with force-reflection only, generalized vibration feedback, and local vibration/force feedback. Lederman and Pawluk argue that intensive coding of stimuli influences roughness perception more than temporal coding of stimuli (20). The comparison of localized to non-localized stimuli for roughness perception might also include the presence or absence of intensive

information (proportional actuation versus binary temporal actuation), or the presence or absence of temporal information (proportional frequency versus single frequency stimulation). The ability of a virtual reality system to control the presentation of intensive and temporal information may yield some useful insights about the perceptual coding of tactile stimuli.

Srinivasan and Chen found that an anaesthetized finger tracking steady-state signals, ramps, and sinusoids in the range 0-1.5 N has a tracking error 50% worse at than that of a non-anaesthetized finger (35). This indicates that cutaneous tactile cues play a role in the control of finger forces in the range significant for the present system. Since the non-tactile PHANToM™ compresses the user's finger in a plastic thimble, a significant reduction in tactile sensitivity might be expected, leading to increased force-control tracking errors. Exactly how much cutaneous sensitivity remains in the thimble-compressed finger remains a question. A force-tracking experiment might compare performance of a subject using the current system or the original PHANToM™ thimble with and without anaesthesia. If an improvement in force tracking performance were noted with the current system, the experiment would highlight a potential advantage of a feedback device capable of precisely-controlled normal forces in addition to vibratory stimuli.

Appendix A. PHANTOM SPECIFICATIONS

the PHANToM Force-Reflecting Haptic Interface

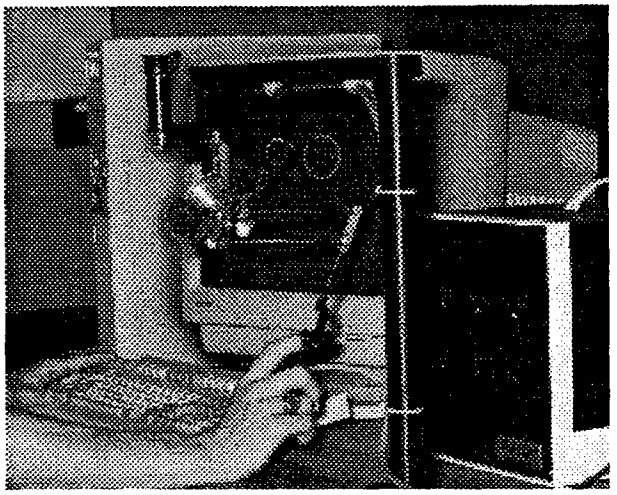

Touching is Believing

The *PHANToM*™ represents the next generation of computer input devices. More than just another passive, 3D mouse, the *PHANToM*™ allows users to actually feel virtual objects. Unlike buzzing tactile stimulators, the *PHANToM*™ actively exterts an external force on the user's finger tip - creating the illusion of interactions with solid virtual objects. Smooth spheres, flat walls, sharp corners, and even texture can be convincingly conveyed to the human haptic system using the device. This is not a bulky exoskeletal device – one simply inserts his or her finger tip into the *PHANToM*™ and interacts with the virtual environment.

High Fidelity

The *PHANToM*™ contains 3 motors which control the x, y, and z forces exerted on the user's finger tip. Mounted on each motor is an optical encoder to determine the x, y, and z position of the user's finger tip. The torque from the motors is transmitted through a proprietary cable transmission to a stiff, light-weight linkage. At the end of this linkage is a passive, 3 degree of freedom gimbal attached to a thimble. The passive gimbal allows the thimble to rotate so that a user's finger tip can then be modelled as a point or frictionless sphere within the virtual world. The device has low friction, low inertia, and no unbalanced weight so movements through free virtual space are unimpeded.

Specifications

Nominal Position Resolution	400 dpi	(0.07mm)
Workspace	5"x7"x10"	(8x17x25 cm)
Backdrive Friction	0.1-0.6 oz.	(0.03-0.18 N)
Maximum Exertable Force	1.9 lbf	(8.5 N)
Closed Loop Stiffness	20 lbs/in	(3.5 N/mm)
Inertia (apparent mass at tip)	<0.22 lbm.	(<100 g)

Versatility

The *PHANToM*™ is best described as a universal force-reflecting interface. In fact, a stylus can be substituted for the thimble. A user can then manipulate the stylus to control the tip of a virtual pencil or paint brush. Users can actually feel the tip of the stylus touch virtual surfaces. The *PHANToM*™ can be used as a high precision force-reflecting master for teleoperation or as a 3 DOF input device for CAD. Artists can mold clay within the computer and surgeons can practice procedures on virtual patients.

SensAble Devices, Inc. 225 Court Street, Vanceburg, Kentucky 41179 606-796-6921

Appendix B. DATA ACQUISITION ELECTRONICS

A wire wrap circuit board mounted to the back plate of the tactile feedback project box contains the data acquisition electronics for the system. Only one of the two designed load cell amplifiers was populated. The load cell amplifier uses an Analog Devices 1B31 strain gauge amplifier chip and can be configured either for the Sensotec Model "D" load cell used in the tactile feedback thimble or the Cooper Model 510 load cell used in the test stand. Figure 33 contains a schematic of the load cell amplifier. To configure it for test stand operation, jumper J1 must be in place to reduce the 1B31 gain resistance to a level appropriate for the Cooper load cell.

The instrumentation amplifier circuit for the LVDT input and solenoid voltage measurement uses a generic quad operational amplifier integrated circuit chip. The schematic for the amplifiers/filters appears in Figure 34. A header plug contains the resistors and capacitors for each amplifier/filter so that gains and cutoffs can be easily adjusted. The LVDT filter begins rolling off at 2 kHz, and the solenoid voltage filter begins rolling off at 5 Hz. The extremely low bandwidth of 5 Hz was selected for noise rejection, and is acceptable because the solenoid voltage measurement is used solely for an overtemperature shutoff

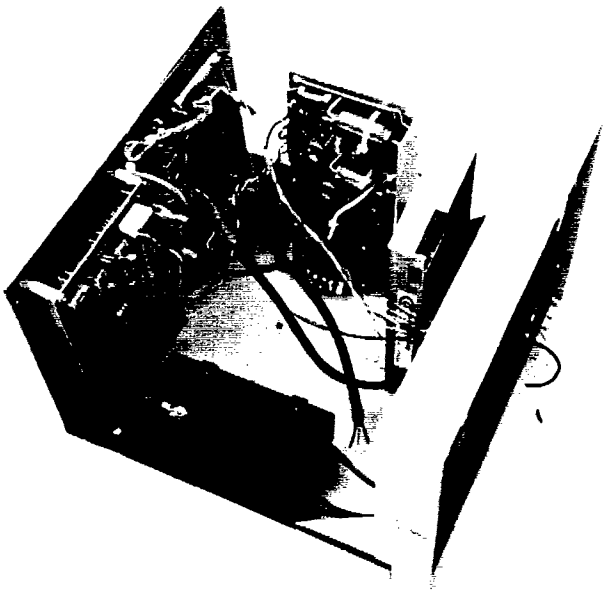

Figure 32. Current Amplifier and Data Conditioning Electronics Box

algorithm presented in Appendix C. The 5 Hz solenoid voltage filter completely eliminates 20 kHz noise from the motor amplifiers that appears as a 25 mV p-p sinusoid when the 2 kHz filter is used, but sharp, higher amplitude voltage spikes remain. Low-capacitance ceramic capacitors may need to be added to the filter to trap this high-frequency artifact.

A shielded cable connects analog signals from the load cell amplifier and quad operational amplifier circuits to a Metrabyte Dash 16/16F analog-to-digital card in the host PC.

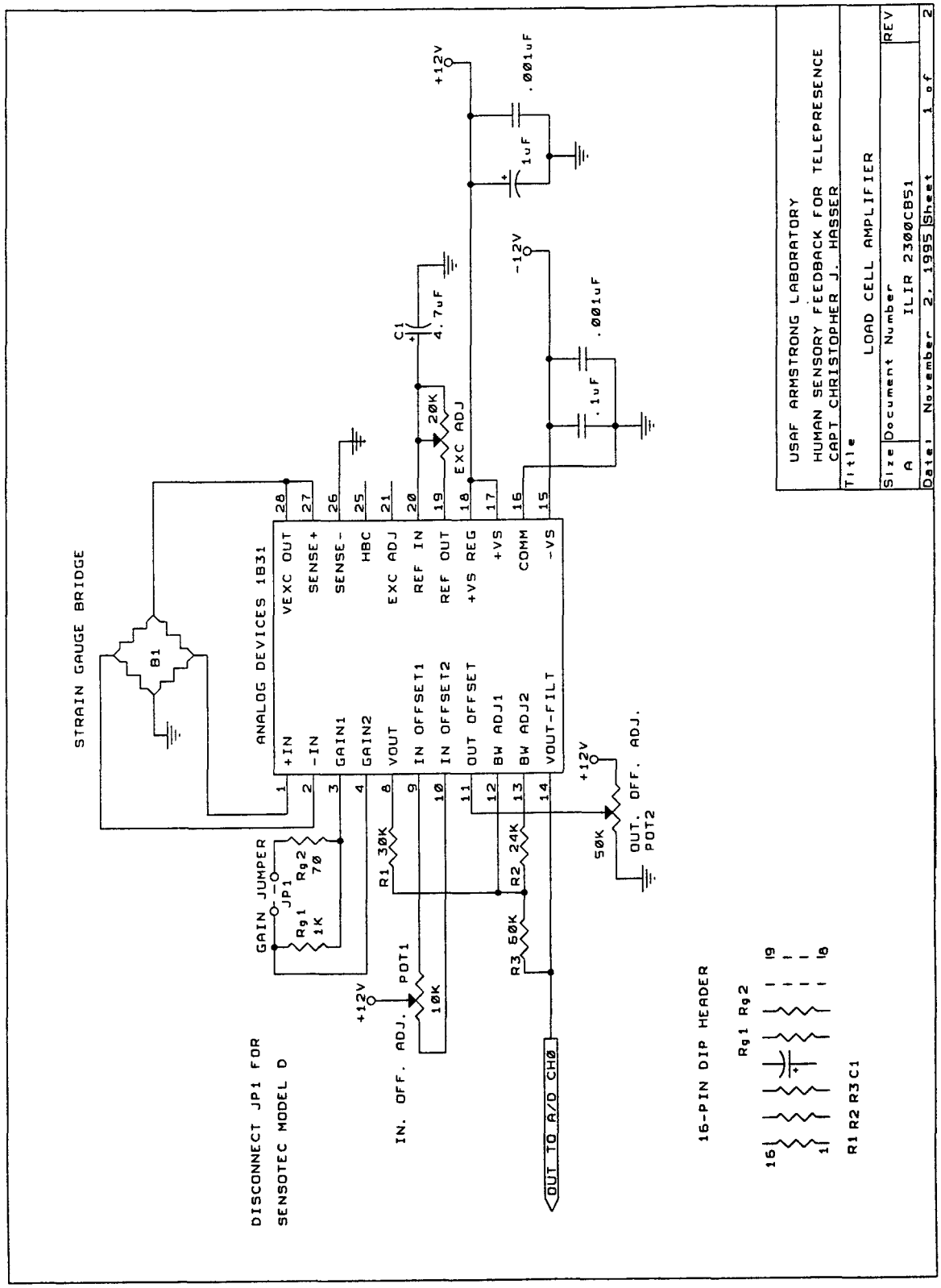

Figure 33. 1B31 Load Cell Amplifier Circuit Schematic

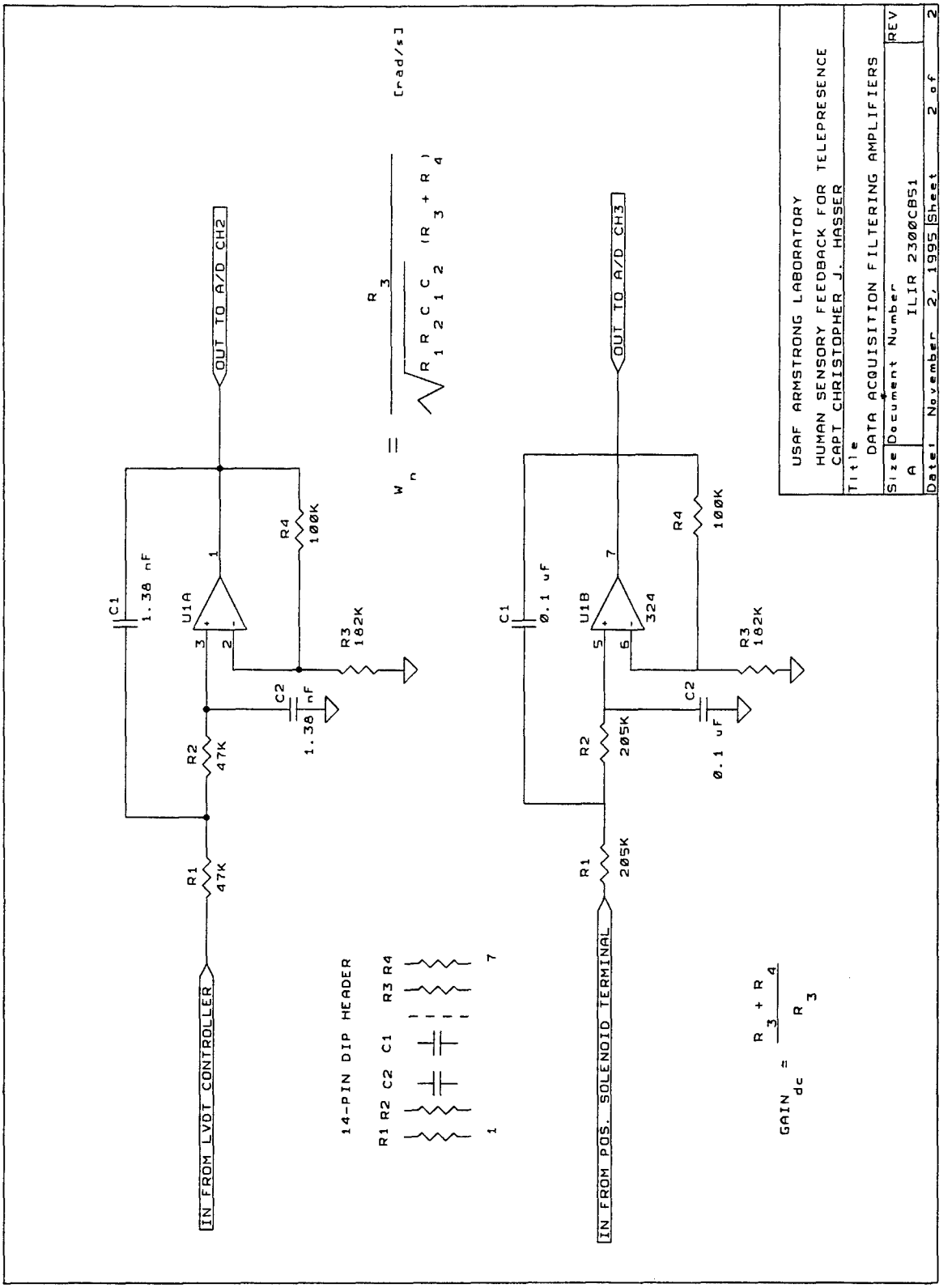

Figure 34. Op-Amp Instrumentation Amplifier Circuit Schematic

Appendix C. SOLENOID TEMPERATURE MEASUREMENT AND MODELING

Two methods may be used to determine the temperature of the solenoid. A thermal model can track the power output to the solenoid and compute an estimated temperature based upon assumed thermal masses and cooling coefficients. This method does not require any A/D conversion. Alternatively, if the current output to the solenoid at a given instant is known and the voltage across the solenoid terminals is measured, the solenoid resistance can be computed using Ohm's law. The temperature of the solenoid coil can be computed using knowledge of the thermal properties of copper or a look-up table provided by the solenoid manufacturer. This method requires A/D conversion to capture the solenoid voltage. Since the system already requires A/D conversion for other functions the latter method was chosen for implementation first.

C.1 Temperature Measurement Based Upon Measured Voltage and Commanded Current

The Copley 303 PWM amplifier that drives the solenoid has a PWM frequency of 20 kHz. In order to monitor the solenoid voltage, one can either sample the amplifier output at a rate much greater than 20 kHz and determine the duty cycle (then multiplying by the supply voltage of 24 V), or the solenoid voltage can be passed through a low-pass filter with high-impedance input (i.e. an op-amp circuit). A filter with a low-impedance input would drag down the frequency response of the solenoid. An existing two-pole op-amp filter with a cutoff of 4 kHz offered a convenient way to filter to a relatively steady signal with ripple of about 100 mV. Unfortunately, this relatively high cutoff frequency left much potential for noise to sneak through. The breakpoint of the filter could be adjusted as low as 2 Hz without problems, since this temperature safety signal was not used for a servo loop, but it proved more expedient to filter the noise in software.

Both the measured solenoid voltage and the calculated output current inject noise into the calculated solenoid resistance so this raw value can have extreme amounts of noise, especially when the solenoid reference force changes frequently. An initial attempt to fil-

ter the noise with a one-pole digital RC network breaking at 4 Hz did not help. Three and five point rectangular FIR (moving average) filters smoothed the signal some, but not enough to make it a reliable temperature indicator. Other traditional filters (e.g. double-pole Butterworth) might have been tried, but a nonlinear gradient-saturating filter offered satisfactory results with little trouble. The filter takes advantage of the fact that temperature will change quite slowly with respect to the sampling rate; any drastic leaps must be caused by noise. If the raw signal jumps by more than a small permissible amount, the algorithm saturates the difference to that permissible amount. The saturation algorithm appears below:

```
if (Rsol > (1.0025*Rsol_z1))
else if (Rsol < (0.9975*Rsol_z1))
   Rsol_filt = 0.9975*Rsol_z1;
else
   Rsol_filt = Rsol;
Rsol_z1 = Rsol_filt;
```

This algorithm repeats every 20th sample (the 2 kHz signal is decimated to produce a filtered 100 Hz signal). So every 10 ms, the temperature signal can change by at most 0.25%.

C.2 Model-Based Temperature Estimation

A simple model estimates the energy input to the solenoid coil (I^2R) and the rate of transfer from the coil through the body, out into the atmosphere.

```
// cu = copper coil, fe = ferrous housing, Rcu = electrical coil resistance
// Rcf = thermal resistance (coil->housing)
// Rfa = thermal resistance (coil->atmosphere)
// Mcu = coil mass, Mfe = housing mass
```

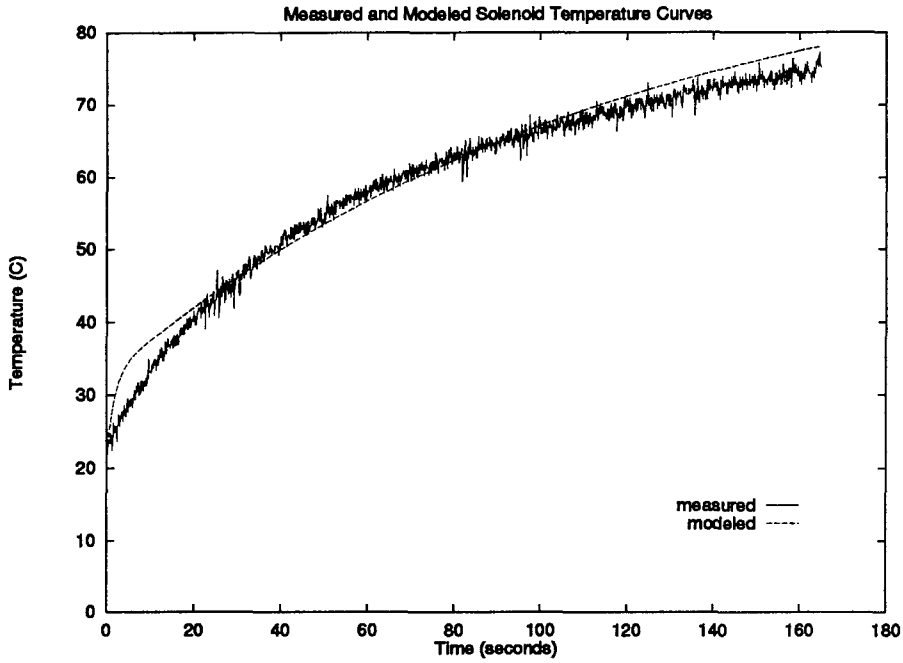

Figure 35. Measured and Modeled Solenoid Temperature Curves (Two-stage Model)

```
Qin = Isol * Isol * Rcu;   /* heat input (Isol = solenoid current) */
Qcf = (Tcu - Tfe) / Rcf;   /* heat flow from copper coil to housing */
Qfa = (Tfe - Tatm) / Rfa;  /* heat flow from housing to atmosphere */
Tcu = Tcu + (Qin - Qcf) / (Mcu * Ccu * (float) 2000); /*coil temp*/
Tfe = Tfe + (Qcf - Qfa) / (Mfe * Cfe * (float) 2000); /*housing temp*/
```

A coil mass of 1.6 g and a housing mass of 17.9 g were estimated, based upon the measured solenoid mass (minus plunger) of 19.5 g, and assuming that the solenoid coil/housing mass ratio is similar to that for the PHANToM™ motors as reported by Massie (30).

Figure 35 compares the performance of the model estimate to the temperature calculated from measured voltage and commanded current.

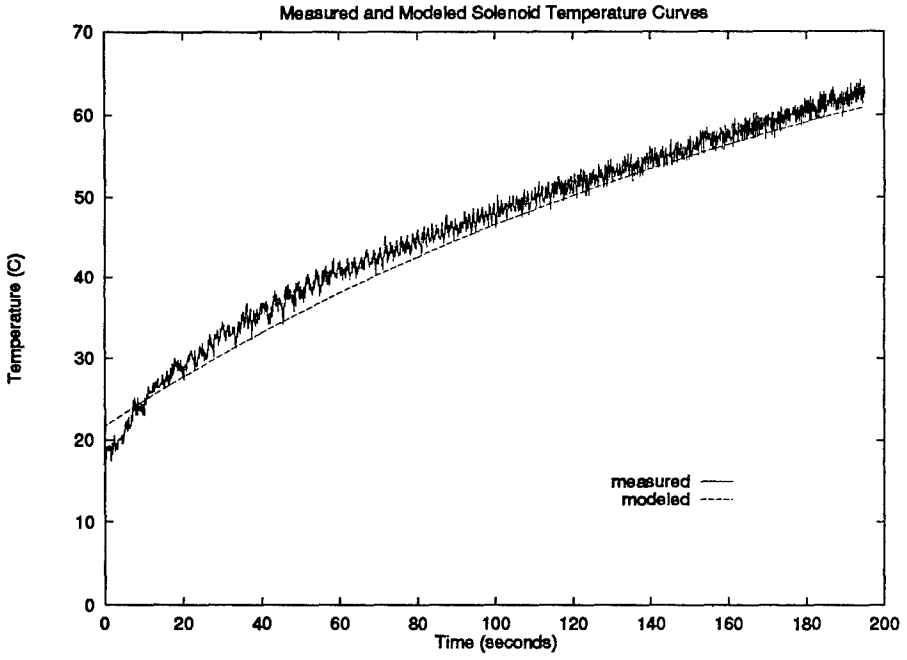

Figure 36. Measured and Modeled Solenoid Temperature Curves (Single-stage Model)

Appendix D. LIST OF SUPPLIERS

ANALOG DEVICES
P.O. BOX 9106
ONE TECHNOLOGY WAY
NORWOOD MA 02062-9106
PHN: 617-329-4700
FAX: 617-326-8703
1B31 strain gauge amplifier IC chip

BORLAND INTERNATIONAL
P.O. BOX 660001
1800 GREEN HILLS ROAD
SCOTTS VALLEY CA 95066-0001
PHN: 408-438-5300
supplied C compiler

COPLEY CONTROLS CORP.
410 UNIVERSITY AVE
WESTWOOD MA 02090-2311
PHN: 617-329-8200
FAX: 617-329-4055
Model 303 PWM servo amplifier

LUCAS CONTROL SYSTEM PRODUCTS
(LEDEX ACTUATION)
P.O. BOX 427
801 SCHOLZ DRIVE
VANDALIA OH 45377-0427
PHN: 513-454-2345
FAX: 513-898-8624
Low-profile solenoids

LUCAS CONTROL SYSTEMS PRODUCTS
1000 LUCAS WAY
HAMPTON VA 23666
PHN: 804-766-1500
FAX: 804-766-4459
LVDT position sensors

METRABYTE CORPORATION
440 MYLES STANDISH BLVD.
TAUNTON MA 02780
PHN: 508-880-3000
FAX: 508-880-0179
Dash 16/16F analog-to-digital PC card

SENSABLE DEVICES INC.
26 LANDSDOWNE ST
CAMBRIDGE MA 02139
PHN: 617-621-0150
FAX: 617-621-0135
PHANToM™, custom gimbal

SENSOTEC
1200 CHESAPEAKE AVENUE
COLUMBUS OH 43212
PHN: 614-486-7723, 800-848-6564
FAX: 614-486-0508
1000 gram Model D donut load cell for tactile
hspace0.15in*thimble*

Appendix E. SOURCE CODE LISTING

E.1 Main Program

```
/*************************************************************************/
/*                                                                       */
/* Main program for "Tactile Feedback for a Force-Reflecting Haptic Display"*/
/*         Master's Thesis, University of Dayton, December 1995          */
/*         Author:  Christopher J. Hasser                                */
/*                  USAF Armstrong Laboratory                            */
/*                  Human Sensory Feedback for Telepresence Project      */
/*                  AL/CFBA, Bldg 441                                    */
/*                  2610 Seventh Street                                  */
/*                  Wright-Patterson AFB OH 45433-7901                   */
/*                  (513)-255-3671                                       */
/*                  c.hasser@ieee.org                                    */
/*                                                                       */
/* This program operates the PHANToM force-reflecting haptic interface   */
/* and a solenoid-driven tactile feedback actuator added to a custom     */
/* orientation-sensing gimbal on the PHANToM for the master's thesis.    */
/*                                                                       */
/* Special thanks go to Marvin Roark, who provided an example interrupt  */
/* service routine for the A/D converter, and to Thomas Massie, who      */
/* provided the kinematic code to interpret the gimbal encoder values.   */
/*                                                                       */
/* The main loop for this program is based partially on a demonstration  */
/* program provided with the PHANToM.  The demonstration code had the    */
/* function of driving the PHANToM motors and setting up a virtual box   */
/* with spheres in it.  The demonstration code had the following header: */
/*                                                                       */
/* Copyright 1993 by SensAble Devices, Incorporated.  All rights reserved */
/*                                                                       */
/*         Author(s):     T. H. Massie         Revision:  1.0            */
/*                                                                       */
/*                Virtual Hemisphere & Eye Program                       */
/*                                                                       */
/*************************************************************************/

#include <graphics.h>
#include <stdlib.h>
#include <conio.h>
#include    <stdio.h>
#include <time.h>
#include    <math.h>
#include <time.h>
```

```
//include two header files below for A/D converter
#include <dos.h>
#include <ctype.h>

#define encoder(axis,offset) \
     ( (inportb((axis<<1)+offset)<<8) ^ (inportb((axis<<1)+1+offset)) )
#define reset_encoder(axis,offset) \
     ((outportb(12+offset, 255-(1<<(axis)))) + (outportb(12+offset,255)))
#define torque(axis,offset,current) {  \
outportb(axis*2+1+offset,(char) (current >> 8)); \
outportb(axis*2+offset,(char) (current & 0xff));}
#define amp_enable(bit,offset) \
        (outportb(12+offset, 63+(bit*128))) /* active low */
#define digital_in(n,offset) ((inportb(12+offset)>>n) & 0x0001)
#define DEV_FAULT(offset) (digital_in(0,offset))
#define STYLUS_SW(offset) (digital_in(1,offset))        /* active low */
// The following two definition lines are included for gimbal encoder code.
#define GIMBAL_ENCODER_COUNTS      512.0
#define GIMBAL_CONVERSION_FACTOR    (-2.0 * M_PI / GIMBAL_ENCODER_COUNTS)

        /* Thermal Constants */

#define  Ccu  385.0     /* Specific Heat of Copper         */
#define Cfe  434.0 /* Specific Heat of Iron           */
#define Mcu  0.0105    /* Mass of the Copper Armature     */
#define Mfe  0.120     /* Mass of the Iron Motor Housing  */
#define Rcu  2.34      /* Electrical Resistance of the Armature  */
#define Rcf  3.10      /* Thermal Resistance, Armature - House   */
#define Rfa  14.0      /* Thermal Resistance, Housing - Atm      */
#define Tatm 25.0      /* Atmospheric Temperature    */
#define Tmax 100.0     /* Shut Down at this temperature(125 max!)*/
#define rate 800.0     /* Average Servo Rate divided by 3 */
#define ApT (10.0/32768.0)   /* conversion factor Amps per Torque tick */

#define T_DATA 0.0005 /*period for data sampling (2000Hz signal is decimated)*/
#define LIMIT 1900    /* maximum number of samples permitted */
#define BIAS_FORCE  0.2  /* bias pressure against finger (Newtons) */

float far k2 = .0002829;
float far k1 = .0002416;
float far l1 = 8250.0;
float far l2 = 8250.0;

// HEADER LINES FOR A/D CONVERSION
extern void das16_init(int,int,int,int);
```

```
void interrupt das16_isr(void);
void interrupt (* save_dasirq_vec)();
interrupt *save_vect;

#define DAS_IRQ  0x0f          /* das16 will be setup to use irq7. */
#define DAS_ADR  0x220         /* das16 set up at hardware address 0x220*/

 long far int   sample_num;
 int   far scan_start,scan_stop;
 float far ad_volts[8] = {0}; // only eight because differential inputs

 float far Fmeas_hx[2000] = {0};
 float far Xmeas_hx[2000] = {0};
 float far Fsol_hx[2000] = {0};
 float far ad_hx[2000] = {0};
 float far Ferr_hx[2000] = {0};
 float far Fmeas,Fref = 0,Xmeas,Ferr,Ferr_z1,Ferr_z2 = 0,Isol;
 long  far Tm[4] = {0}, Tm_old[4] = {0};
 float far sol_temp = 20.0;

// END OF HEADER LINES FOR A/D CONVERSION

int far base_addr;
char far datafile[20];
FILE *df;

void servo_loop(int base_addr);
int temp_check(float Tcu[], float Tfe[], long Tm[], int axis);
void get_stylus_matrix(float T[4][4], int base_addr);
float ab(float x);

// VARIABLES FOR A/D CONVERSION
  int temp,int8259a;

main()
{
  int j;

  int axis;
//  int base_addr;
  char input[50];
  long final_pos;
  unsigned char max_vel;
  unsigned int acc;
  int active_axes;
```

```
  int running_flag;
  char inchar;
  double N_sum = 0; // sum of noise squared
  double S_sum = 0; // sum of signal squared

int gdriver=DETECT,gmode,errorcode;
int midx,midy;
initgraph(&gdriver,&gmode,"");
errorcode=graphresult();
if(errorcode != grOk)
  {
  printf("error:%s\n",grapherrormsg(errorcode));
  printf("press any key:");
  getch();
  exit(1);
  }

// Open data file
sprintf(datafile,"solenoid.dat");
if ((df = fopen(datafile,"w")) == NULL) /* cannot create file */
  printf("ERROR:  Could not create data file.");

clrscr();

base_addr = 0x300;

cleardevice();

printf("\n\nPress return to continue");
getch();
printf("\n\n");

// SET UP A/D CONVERSION
   save_dasirq_vec = getvect(DAS_IRQ);
   printf ( "DAS_IRQ %x interrupt = %Fp address\n",DAS_IRQ,save_dasirq_vec);
   disable();
   setvect(DAS_IRQ,das16_isr);  /* das16 interrupt service routine */
   enable();
   // The first two parameters of the initialization command, below
   // set the sampling interval of the A/D converter.  Multiply them
   // together, and use to divide the 1 MHz clock; so 25,10 would be 4kHz.
   // On 28 Jun 95, CJH changed to 25,20 for 2kHz since there was too much
   // code in ISR for it to do it at 4kHz (I think).
   das16_init(25,20,0,3);  /* initialize and start das16 */
   int8259a=inportb(0x21);
```

```
   temp=inportb(DAS_ADR+8);
   printf("\nAfter init: SR=%x samples %ld 8259=%x\r", \
        temp,sample_num,int8259a);
// END OF A/D CONVERSION SETUP

/* set torques to zero */
  torque(0,base_addr,32768);
  torque(1,base_addr,32768);
  torque(2,base_addr,32768);
  torque(3,base_addr,32768);
  amp_enable(0,base_addr);

/* start the servo loop! */
  servo_loop(base_addr);

/* set torques to zero, disable amplifiers, clean up */
  torque(0,base_addr,32768);
  torque(1,base_addr,32768);
  torque(2,base_addr,32768);
  torque(3,base_addr,32768);
  amp_enable(1,base_addr);

  // CLEAN UP FOR A/D CONVERSION CODE
   disable();
   outportb(DAS_ADR+10,1);
   /* disable irq7 in the interrupt controller */
   outportb(0x21,0x80 & inportb(0x21));
   /* reset the control register */
   outportb(DAS_ADR+9,0);
   enable();

printf("sample_num = %ld",sample_num);

     for (j=0;((j<(sample_num/(2000*T_DATA)))&&(j<2000));j++)
     {
     fprintf(df,"%f\t%f\t%f\t%f\t%f\n", \
             j*T_DATA,Xmeas_hx[j],Ferr_hx[j],Fmeas_hx[j],ad_hx[j]);
     if (j>500){///((int) 1/T_DATA)) {/*omit first second from noise calc.*/
     N_sum += Ferr_hx[j] * Ferr_hx[j];
     Xmeas_hx[j] -= 0.5;
     S_sum += Xmeas_hx[j]*Xmeas_hx[j]; //Xmeas now being used to store Fref
      }
     }
   printf("\n Signal-to-noise ratio = %f\n",S_sum/N_sum);
```

```
// close data file
   fclose(df);

   exit(0);
   return 0;
// END OF A/D CONVERSION CLEANUP

}

float ab(float x)
{
  if (x>=0) return (x);
    else return (-x);
}

void servo_loop(int base_addr)
{
   unsigned char command[4];
long int elapsed,runs=0;
   int axis;
   float theta_hack;
   int n;
   float forcex,forcey,forcez,theta_J1,theta_J2,theta_J23;
   float stiffness=1000.0, x, y, z, cubex[10], cubey[10], cubez[10], size[10];
   float s23,c23,s1,c1,clg,slg;
   float spherex[]={ 8250.0,   8250.0,  8250.0};
   float spherey[]={ 0.0,  1500.0,  1000.0};
   float spherez[]={ -9300.0,  -7500.0, -7500.0};
   float R[]    ={  1000.0, 1000.0, 700.0};
   float mag,w,xc,yc,zc;
float gradual;
float Tcu[]={Tatm, Tatm, Tatm};
float Tfe[]={Tatm, Tatm, Tatm};
long  Tm[3];
   time_t t;
   // GIMBAL CONVERSION CODE TRANSFORM MATRIX:
   float T[4][4] = {0};
   int i,j,k;
   // world frame and gimbal frame vectors for tactile fingertip
   float wP[4],gP[4]={0,0,1,1};
   float mystic_coeff;

/* delay to allow amplifier box to come on */
for(elapsed=0;(elapsed<9000000);elapsed++);
```

```
t = time(NULL);
elapsed=t;

 while (!kbhit() & !DEV_FAULT(base_addr))
  {
   // Don't overwrite past boundaries of history arrays
//   if (sample_num>LIMIT) break;

   runs=runs+1;

   theta_J1  = (float) k1 * (float) (encoder(0,base_addr));
   theta_J2  = -1.0 * (float) k2 * (float) (encoder(2,base_addr));
   theta_J23 = -1.57 - (float) k2 * (float) (encoder(1,base_addr));

   s23=sin(theta_J23);
   c23=cos(theta_J23);
   c1=cos(theta_J1);
   s1=sin(theta_J1);
   clg=(cos(theta_J2)*l1+l2*c23);
   slg=(sin(theta_J2)*l1+l2*s23);

   x=c1*clg;
   y=s1*clg;
   z=slg;

   forcex=0.0; forcey=0.0; forcez=0.0;

//  Call the GIMBAL CONVERSION kinematics code here:
   get_stylus_matrix(T,base_addr);

  // now compute wP=T*gP
  for (i=0;i<3;i++)
  {
    wP[i]=0.0;
    for (k=0;k<3;k++)
    {
     wP[i] = wP[i] + (T[i][k]*gP[k]);
    }
  }

   /* this is the BIG BOX ROUTINE */

   if (x<5250.0) forcex=(5250.0-x)*.1;
     else if (x>11250.0) forcex=(11250.0-x)*.1;
   if (y>6000.0) forcey=(6000.0-y)*.1;
```

```
    else if (y<-6000.0) forcey=(-6000.0-y)*.1;
   if (z>-3750.0) forcez=(-3750.0-z)*.1;
 else if (z<-9300.0) forcez=(-9300.0-z)*.1;

   zc=(sin((double)x/40.0)*sin((double)y/40.0))*40.0;
   if (z>(-3750.0+zc)) forcez=(-3750.0+zc-z)*.1;
 else if (z<(-9300.0+zc)) forcez=(-9300.0+zc-z)*.1;

   /* spheres */
  for(n = 0; n < 3; n++)
  {
xc = (x-spherex[n]);
yc = (y-spherey[n]);
zc = (z-spherez[n]);
w=xc*xc+yc*yc+zc*zc;
if (w<(R[n]*R[n]))
{
mag=(R[n]/sqrt(w)-1)*.1;
forcex=forcex+mag*xc;
forcey=forcey+mag*yc;
forcez=forcez+mag*zc;
}
  }

   // Determine force to be applied to solenoid.  Use the cross product
   // of the PHANToM force and the solenoid (fingertip) orientation.

   Fref = BIAS_FORCE + 0.1*(wP[0]*forcex + wP[1]*forcey + wP[2]*forcez);
   if (Fref < BIAS_FORCE) Fref = BIAS_FORCE;

   gradual=1.0;
   if (runs<10000) gradual=(float) runs * (float) runs/100000000.0;

Tm[0]=(long)(gradual*256.0*k1*(-s1*clg*forcex+c1*clg*forcey));
Tm[2]=(long) \
      (gradual*256.0*k2*(-c1*l2*s23*forcex-s1*l2*s23*forcey+l2*c23*forcez));
Tm[1]=-Tm[2]+(long) \
      (gradual*256.0*k2*(-c1*slg*forcex-s1*slg*forcey+clg*forcez));

if (Tm[0]>30000) {printf("Tm[0] = %ld at run %ld and sample %ld\t \
  forcex=%f\n",Tm[0],runs,sample_num,forcex); Tm[0]=Tm_old[0];}
if (Tm[0]<-30000) Tm[0]=Tm_old[0];
if (Tm[1]>30000) Tm[1]=Tm_old[1];
if (Tm[1]<-30000) Tm[1]=Tm_old[1];
if (Tm[2]>30000) {printf("Tm[2] = %ld at run %ld and sample %ld\t \
```

```
  forcex=%f\n",Tm[2],runs,sample_num,forcex); Tm[2]=Tm_old[2];}
if (Tm[2]<-30000) Tm[2]=Tm_old[2];

if (temp_check(Tcu,Tfe,Tm,(runs%3))) break;
//   if (sol_temp > 70) {
//   printf("\n\n\n OVERTEMPERATURE SHUTOFF (T=%4.2f C).  \
     ALLOW SOLENOID TO COOL BEFORE PROCEEDING \n\n\n",sol_temp);
          //break;
  //        }

   torque(0,base_addr,(long) (Tm[0] +32768.0));
   torque(1,base_addr,(long) (Tm[2] +32768.0));
   torque(2,base_addr,(long) (Tm[1] +32768.0));
 }
 t = time(NULL);
 elapsed=t-elapsed+1;
// closegraph();
 printf("average servo rate %ld Hz\n",(runs/elapsed));
 printf("Fref = %f\n",Fref);
} // end of servo function

/* ------------------------------ */
/*     Temperature tracking       */
/* ------------------------------ */
/*  Pass it motor torque          */
/*  will update Temp of Motor     */
/*  Returns a 1 if too hot   */
/* ------------------------------ */

int temp_check(float Tcu[], float Tfe[], long Tm[], int axis)
{
 float Qcf,Qin,Qfa; /* Heat flows */

Qin = ApT * ApT * (float) Tm[axis] * (float) Tm[axis] * Rcu;
Qcf = (Tcu[axis] - Tfe[axis] ) / Rcf;
Qfa = (Tfe[axis] - Tatm) / Rfa;
Tcu[axis] = Tcu[axis] + (Qin - Qcf) / (Mcu * Ccu * (float) rate);
Tfe[axis] = Tfe[axis] + (Qcf - Qfa) / (Mfe * Cfe * (float) rate);
return (Tcu[axis]>Tmax);
}


void get_stylus_matrix(float T[4][4], int base_addr)
{
//this routine assumes that the following have
```

```
//been defined globally:
//
//   #define l1    8250.0
//   #define l2    8250.0
//   #define k2    0.0002829
//   #define k1    0.0002416
   //   #define encoder(axis,offset) \
   //     ( (inportb((axis<<1)+offset)<<8) ^ (inportb((axis<<1)+1+offset)) )
   //   #define GIMBAL_ENCODER_COUNTS      512.0
//   #define GIMBAL_CONVERSION_FACTOR  (-2.0 * M_PI /GIMBAL_ENCODER_COUNTS)
//

// some of these variables names are more "historical" than "logical"
static float theta_J1, theta_J2, theta_J23;
   static float s23, c23, c1, s1, clg, slg;
   static float ce1,ce2,ce3,se1,se2,se3;
   static float N[4][4], M[4][4];
   static float theta_E[3];
   static float p[3];
   static int i,j,k;

// same code as GET_XYZ
// if code has to be really fast, we would avoid recalculating
// this part of the kinematics

// angles of PHANToM links
// theta_J23 is angle of last link wrt to ground
theta_J1  = k1 * (float) (encoder(0,base_addr));
theta_J2  = -k2 * (float) (encoder(2,base_addr));
theta_J23 = -M_PI/2.0 - k2 * (float) (encoder(1,base_addr));

   s23=sin(theta_J23);
   c23=cos(theta_J23);
   c1=cos(theta_J1);
   s1=sin(theta_J1);
   clg=(cos(theta_J2)*l1+l2*c23);
   slg=(sin(theta_J2)*l1+l2*s23);

// p[] contains the position vector for the PHANToM endpoint
p[0]=c1*clg;
   p[1]=s1*clg;
   p[2]=slg;

// note that we add 90 degrees to theta_J23 because
// last link of PHANToM is 90 degrees to the horizontal when it is in
```

```
// the neutral position, but we don't
// want to rotate the gimbal frame 90 degrees

theta_J23 = -theta_J23 - M_PI/2.0;
   s23=sin(theta_J23);
   c23=cos(theta_J23);

  // here we change encoder values to gimbal angles

  theta_E[0]= (float) GIMBAL_CONVERSION_FACTOR * \
      (float) (encoder(3,base_addr));
  theta_E[1]= (float) GIMBAL_CONVERSION_FACTOR * \
      (float) (encoder(4,base_addr));
  theta_E[2]= (float) GIMBAL_CONVERSION_FACTOR * \
      (float) (encoder(5,base_addr));

  // gimbal angles sines and cosines

  ce1=cos(theta_E[0]);
  ce2=cos(theta_E[1]);
  ce3=cos(theta_E[2]);
  se1=sin(theta_E[0]);
  se2=sin(theta_E[1]);
  se3=sin(theta_E[2]);

  // matrix to transform points from Stylus frame into Link frame
  // first index denotes row, second index denotes column

  N[0][0]=ce1*ce2;
  N[0][1]=ce1*se2*se3-se1*ce3;
  N[0][2]=ce1*se2*ce3+se1*se3;
  N[0][3]=0.0;

  N[1][0]=se1*ce2;
  N[1][1]=se1*se2*se3+ce1*ce3;
  N[1][2]=se1*se2*ce3-ce1*se3;
  N[1][3]=0.0;

  N[2][0]=-se2;
  N[2][1]=ce2*se3;
  N[2][2]=ce2*ce3;
  N[2][3]=0.0;

  N[3][0]=0.0;
  N[3][1]=0.0;
```

```
  N[3][2]=0.0;
  N[3][3]=1.0;

  // matrix to transform points from Link frame into World frame

  M[0][0]=c23*c1;
  M[0][1]=-c23*s1;
  M[0][2]=s23;
  M[0][3]=p[0];

  M[1][0]=s1;
  M[1][1]=c1;
  M[1][2]=0.0;
  M[1][3]=p[1];

  M[2][0]=-s23*c1;
  M[2][1]=s23*s1;
  M[2][2]=c23;
  M[2][3]=p[2];

  M[3][0]=0.0;
  M[3][1]=0.0;
  M[3][2]=0.0;
  M[3][3]=1.0;

  // now compute T=MN
  for (i=0;i<4;i++)
  {
   for (j=0;j<4;j++)
   {
    T[i][j]=0.0;
    for (k=0;k<4;k++)
    {
     T[i][j] = T[i][j] + (M[i][k]*N[k][j]);
    }
   }
  }
  // done.  Now T contains the matrix to take any point in the
  // stylus frame and express it in the world frame, taking
  // into accout the rotation of the gimbal axes and the translation
  // of the end point by the PHANToM haptic interface.
}
```

E.2 Initialization Routine

```
#include <dos.h>
#define DAS_ADR  0x220        /* das16 set up at hardware address 0x220*/
extern far long int   sample_num;
extern far int scan_start,scan_stop;

/* das16 mux scan register */

/* das16 status register info */

   /* a write to the status register clears the interrupt request
      and re-enables it. */

/* das16 control register info */
#define DAS16_CR_S_TIMER  3    /* start a/d conversion on timer output */
#define DAS16_CR_L_IRQ    0x70 /* irq 7 */
#define DAS16_CR_INTE     0x80 /* enable interrupt */

/* das16 counter info */
#define DAS16_CTR_M_RG    4    /* rate generator */
#define DAS16_CTR_RL_LO   0x10 /* write lo byte to 16 bit counter*/
#define DAS16_CTR_RL_HI   0x20 /* write hi byte to 16 bit counter*/
#define DAS16_CTR_RL_LOHI 0x30 /* write lo then hi byte to 16 bit counter*/
#define DAS16_CTR_SC_0    0    /* 16 bit counter 0 */
#define DAS16_CTR_SC_1    0x40 /* 16 bit counter 1 */
#define DAS16_CTR_SC_2    0x80 /* 16 bit counter 2 */
#define DAS16_CTR_SC_RB   0xc0 /* 16 bit counter read back command*/

void das16_init(int count1, int count2,
                int start_ad,int stop_ad)     /* initialize DAS board */
{
   unsigned int xl,xh;
   sample_num=0;
   scan_start=start_ad;
   scan_stop=stop_ad;
   disable();

   /* set up the counter control register */
   outportb(DAS_ADR+15,DAS16_CTR_M_RG|DAS16_CTR_RL_LOHI|DAS16_CTR_SC_1);
   printf("\nccr1=%x",DAS16_CTR_M_RG|DAS16_CTR_RL_LOHI|DAS16_CTR_SC_1);

   /* set up the counter control register */
   outportb(DAS_ADR+15,DAS16_CTR_M_RG|DAS16_CTR_RL_LOHI|DAS16_CTR_SC_2);
   printf("\nccr2=%x",DAS16_CTR_M_RG|DAS16_CTR_RL_LOHI|DAS16_CTR_SC_2);
```

```
    /* setup the counter registers */

    xl=count1;
    xh=count1>>8;    /* right shift count by 8 bits (divide) */

    outportb(DAS_ADR+13,xl);          /* counter 1 low byte */
    outportb(DAS_ADR+13,xh);          /* counter 1 high byte */

    /* setup the counter registers */

    xl=count2;
    xh=count2>>8;    /* right shift count by 8 bits (divide) */

    outportb(DAS_ADR+14,xl);         /* counter 2 low byte */
    outportb(DAS_ADR+14;xh);          /* counter 2 high byte */

    /* set up the a/d mux scan register */

    outportb(DAS_ADR+2, ((scan_stop<<4) + scan_start) );
                                      //assuming start and stop scan < 8

                        /* valid numbers are 0-7 for start and
                           00-70 for stop. 8 bit register. To do a
                           single channel- start and stop = same channel
                           start is lower 4 bits, stop is upper 4 bits.
                        */

    outportb(DAS_ADR+8,0); /* re-enable the das16 interrupt */

    /* enable irq7 in the interrupt controller */
    outportb(0x21,~0x80 & inportb(0x21));

    /* setup the control register */
    outportb(DAS_ADR+9,DAS16_CR_INTE|DAS16_CR_L_IRQ|DAS16_CR_S_TIMER);
    printf("\nctr=%x",DAS16_CR_INTE|DAS16_CR_L_IRQ|DAS16_CR_S_TIMER);

    /* enable the counter timer */
    outportb(DAS_ADR+10,1);

    enable();

} /* disabled */
```

E.3 Interrupt Service Routine

```
#include  <math.h>

#define DAS_ADR  0x220        /* das16 set up at hardware address 0x220*/
#define Kp       .675
#define Ti       0.0076
#define Kd       0
#define T_sample 0.0005
#define Gain     Kp
#define Gain_p   Gain*(1+T_sample/2/Ti)
#define Beta     (2*Ti-T_sample)/(2*Ti+T_sample)
#define DEC      1  // save every DECth data point
#define LIMIT    1900 // with 2000 hx array, LIMIT is < 2000*DEC
#define RATE_DIVISOR  2000/2000  // 2000/rate.  Rate is desired in Hz
#define RECORD_DATA  0

void interrupt das16_isr()
{
extern far long int   sample_num;
extern far int scan_start,scan_stop;
extern far float ad_volts[8]; // only eight because differential inputs
extern far float Fmeas_hx[],Xmeas_hx[],Fsol_hx[],ad_hx[],Ferr_hx[];
extern far float Fmeas,Fref,Xmeas,Ferr,Ferr_z1,Ferr_z2,Isol;
extern far long  Tm[4];
extern far int   base_addr;
extern far float sol_temp;

     int i,value,xl,xh,Ge,Gf;
     static float ad_volts_z1[8] = {0},ad_volts_z2[8] = {0};
     // above variable is ad_volts, delayed by one sample
     static float Rsol_z1 = 15.4, Rsol_z2 = 0, Rsol_z3 = 0, Rsol_z4=0;
     float kx2,kx1,kx0;  // coefficients for current vs. force eq.
     float FvP,IvF,Fsol,Rsol=16.7,Rsol_filt=16.7,Ferr_int = 0,Kiff=0;
     float Isol_z1 = 0;
     static float F = 0;
     int hx_index;
     long Isol_int,Rsol_int,Fmeas_int;
     static long Rsol_z1_int = 167000, Rsol_filt_int = 167000;
     static float Kiff_meas[20]={5,5,5,5,5,5,5,5,5,5,5,5,5,5,5,5,5,5,5,5};

     /* if we got here, it was because the a/d caused an interrupt */
     /* so get the a/d value */

     sample_num++;
```

```
      for(i=scan_start;i<=scan_stop;i++)
      {
         /* get the a/d values */
         xl=inportb(DAS_ADR);   /* lower byte */
         xh=inportb(DAS_ADR+1); /* upper byte */
         value=(xh*16)+(xl/16);

         ad_volts[i]= (float)(value-2048)/2048.*5.;

         if(i<scan_stop) // start the next scan
         {
            outportb(DAS_ADR,0); // start the a/d conversion
            while(inportb(DAS_ADR+8 && 0x40)){}//wait until (end of conversion)
         }
      }
      outportb(DAS_ADR+8,0); /* re-enable the das16 interrupt */

      outportb(0x20,0x20); /* non specific eoi*/

//    END OF A/D ACQUISITION.  Now do servo calculations and save hx vectors
//      ad_volts[2] = 0.785*ad_volts[2] + 0.105*ad_volts_z1[2];
//      ad_volts_z1[2] = ad_volts[2];

      // Fmeas equation below is for new "donut" load cell
      Fmeas = ((77.821*ad_volts[0] + 361.868)/101.937) + .2;  // (Newtons)
      Xmeas = 0.0386*ad_volts[2] + .091;

//  Determine current command to solenoid
      Fsol = 1*Fref; // 0.1 lbs
//    Fsol = .5 + 0.2*sin(6.28*sample_num/10);
//      if (sample_num > 1000) Fsol = 2; else Fsol=0;
//      if (Fsol>0) Fsol=0.15; else Fsol = 0;
      Ferr = Gain_p*(Fsol - Fmeas);

//Isol = 0.275 + 0.275*sin(6.28*sample_num/4000);
Fmeas_int = Fmeas * 10000;
// PREDICT KIFF USING CURVE
//if (Fmeas_int >= 800)
//  Kiff = .4/Fmeas;
//else                // if F<0.08N, then saturate Kiff at 5
//  Kiff = 5;

// CALCULATE KIFF USING MEASURED DATA
if (Fmeas_int >= 800)
  Kiff_meas[sample_num%20] = Isol/Fmeas;
```

```
else                    // if F<0.08N, then saturate Kiff at 5
  Kiff_meas[sample_num%20] = 5;
Kiff = 0;
for(i=0;i<=20;i++)
  Kiff += Kiff_meas[i];
// For some really strange reason, the computer adds the value for
// Rsol to Kiff before dividing by 20.  Rsol has *nothing* to do with
// this calculation, but is subtracted out below as a patch to the problem.
Kiff = (Kiff-Rsol)/20;

Isol = Kiff*Ferr + F;
//Isol = 0.22 + (sin((float) 6.28*sample_num/2000))*0.22;
     //  For some odd reason, testing floating point variables like
     //  Isol in "if" statements caused noisy spikes in the Tm[] values.
     //  After many hours of angst, this problem could not be solved.
     //  The patch is to test on scaled integers.  In the saturation
     //  code below, I was able to leave the Isol = 1 and Isol = 0
     //  lines as floats without a problem.

     Isol_int=Isol * 10000;
     if (Isol_int > 8000) Isol = 0.8;
     if (Isol_int < 0) Isol = 0;

     F = Beta*F + (1-Beta)*Isol;
     Tm[3] = -3139*Isol;
     if (Tm[3]<-3139) Tm[3] = -3139;
     if (Tm[3]>0) Tm[3] = 0;

     outportb(3*2+1+base_addr,(char) ((long) (Tm[3] +32768.0) >> 8));
     outportb(3*2+base_addr,(char) ((long) (Tm[3] +32768.0) & 0xff));
     // Calculate solenoid resistance by dividing measured solenoid
     // voltage by commanded current through solenoid.
     if (Isol_int != 0)
       Rsol = 48000*ad_volts[3]/Isol_int;
       // 48000 = 10000*4.8*fudge, where 4.8 is 24/5 A-D scaling,
       // and "fudge" is fudge factor to begin with correct resistance
     Rsol_int = 10000*Rsol;
     if (Rsol_int > 220000) Rsol_int = 220000;
     if (Rsol_int < 140000) Rsol_int = 140000;

//  Save every 20th sample set to history vectors
     Ge=!(sample_num % 20);
     if ((sample_num<39000)&&(Ge))
        {
//if (Rsol_int > (1.0025*Rsol_z1_int))
```

```
//   Rsol_filt_int = 1.0025*Rsol_z1_int;
//else if (Rsol_int < (0.9975*Rsol_z1_int))
//   Rsol_filt_int = 0.9975*Rsol_z1_int;
//else
//   Rsol_filt_int = Rsol_int;
//Rsol_z1_int = Rsol_filt_int;
//Rsol = (float) Rsol_int/10000;
//Rsol_filt = (float) Rsol_filt_int/10000;
//Rsol_z1 = (float) Rsol_z1_int/10000;
//sol_temp = (float) 20 + ((Rsol_filt/16.7 - 1)/0.00393);

//Rsol_filt = (Rsol + Rsol_z1 + Rsol_z2 + Rsol_z3 + Rsol_z4)/5;
//Rsol_filt = 0.012566*Rsol + 0.9875*Rsol_z1;

//Rsol_z4 = Rsol_z3;
//Rsol_z3 = Rsol_z2;
//Rsol_z2 = Rsol_z1;
        }

      Gf=!(sample_num % DEC);
      if ((sample_num<LIMIT)&&(Gf)&&RECORD_DATA)
        {
        hx_index = sample_num/DEC;
        Xmeas_hx[hx_index] = Fsol;//Isol;//Xmeas;
        // line below should equal Ferr.  Change to Ferr_int for debugging
        Ferr_hx[hx_index] = Isol/Fmeas;//Ferr/Gain_p;
        Fmeas_hx[hx_index] = Fmeas;
        ad_hx[hx_index] = Kiff;//ad_volts[0];
        if ((hx_index)>199)
          Ferr_int = Ferr_int - Ferr_hx[hx_index-200];
        Fsol_hx[hx_index] = Fsol;
        }
}
```

Bibliography

1. J. C. Bliss, J. W. Hill, and B. M. Wilber. Tactile Perception Studies Related to Teleoperator Systems. NASA Technical Report CR-1775, Stanford Research Institute, Menlo Park CA, April 1971.
2. R. A. Browse and M. L. McDonald. Using Tactile Information in Telerobotics. *IEEE Trans. on Systems, Man, and Cybernetics*, 22(5):1205–1210, September/October 1992.
3. E. Y. Chen and B. A. Marcus. EXOS Hand Exoskeleton Haptic Display. In *ASME Winter Annual Meeting–Session on Haptic Interfaces for Virtual Environment and Teleoperator Systems*, Chicago, November 1994.
4. D. W. Clarke. PID Algorithms and Their Computer Implementation. *Trans Inst M C*, 6(6):305–316, Oct-Dec 1984.
5. J. J. Craig. *Introduction to Robotics: Mechanics and Control.* Addison-Wesley, 2nd edition, 1989.
6. EXOS. SAFiRE Phase II Quarterly Report. SBIR Contract for NASA, October-December 1993.
7. R. J. Gulati. Determination of mechanical properties of the human fingerpad, *in vivo*, using a tactile stimulator. Master's thesis, Boston University, Boston MA, 1994.
8. C. J. Hasser and J. M. Weisenberger. Preliminary Evaluation of a Shape-Memory Alloy Tactile Feedback Display. In *ASME Winter Annual Meeting–Session on Haptic Interfaces for Virtual Environment and Teleoperator Systems*, pages 73–80, New Orleans LA, November 1993.
9. R. D. Howe. A Force-Reflecting Teleoperated Hand System for the Study of Tactile Sensing in Precision Manipulation. In *Proc. of the IEEE Int. Conf. on Robotics and Automation*, Nice France, May 1992.
10. R. D. Howe, W. J. Peine, D. A. Kontarinis, and J. S. Son. Remote Palpation Technology. *IEEE Eng. in Med. and Bio. Mag.*, May-June 1995.
11. B. M. Jau, M. A. Lewis, and A. K. Bejczy. Anthropomorphic Telemanipulation System in Terminus Control Mode. In *Proc. of RoManSy '94: The Tenth CISM-IFToMM Symp. on Theory and Practice of Robots and Manipulators*, 1994.
12. R. S. Johansson, U. Landstrom, and R. Lundstrom. Responses of Mechanoreceptive Afferent Units in the Glabrous Skin of the Human Hand to Sinusoidal Skin Displacements. *Brain Research*, 244:17–25, 1982.
13. R. S. Johansson and G. Westling. Signals in Tactile Afferents From the Fingers Eliciting Adaptive Motor Responses During Precision Grip. *Experimental Brain Research*, 66:141–154, 1987.
14. K. O. Johnson and S. S. Hsiao. Neural Mechanisms of Tactual Form and Texture Perception. *Annu. Rev. Neurosci.*, 15:227–250, 1992.
15. K. Kaczmarek and P. Bach y Rita. Tactile Displays. In W. Barfield and T. Furness, editors, *Advanced Interface Design and Virtual Environments.* Oxford University Press, 1993.

16. D. A. Kontarinis and R. D. Howe. Display of High-Frequency Tactile Information to Teleoperators. In *Telemanipulator Technology and Space Telerobotics*, Boston MA, September 1993. SPIE vol. 2057.

17. D. A. Kontarinis and R. D. Howe. Tactile Display of Contact Shape in Dextrous Telemanipulation. In *ASME Winter Annual Meeting–Session on Haptic Interfaces for Virtual Environment and Teleoperator Systems*, New Orleans LA, November 1993.

18. D. A. Kontarinis and R. D. Howe. Tactile Display of Vibratory Information in Teleoperation and Virtual Environments. *Presence: Teleoperators and Virtual Environments*, 1995. MIT Press.

19. D. A. Kontarinis, J. S. Son, W. J. Peine, and R. D. Howe. A Tactile Shape Sensing and Display System for Teleoperated Manipulation. In *IEEE Conf. on Robotics & Automation*, 1995.

20. S. J. Lederman and D. T. Pawluk. Lessons From The Study of Biological Touch for Robot Tactile Sensing. In H. R. Nicholls, editor, *Advanced Tactile Sensing for Robotics.* World Scientific Pub., River Edge NJ, 1992.

21. J. M. Loomis and S. J. Lederman. Tactual Perception. In K. R. Boff, L. Kaufman, and J. P. Thomas, editors, *Handbook of Human Perception and Performance — Volume II, Cognitive Processes and Performance*, pages 31–1 – 31–41. Wiley & Sons, 1986.

22. M. Massimino and T. B. Sheridan. Variable Force and Visual Feedback Effects On Teleoperator Man-machine Performance. In *NASA Conference on Space Telerobotics*, Pasadena CA, 31 January - 2 February 1989.

23. T. J. Moore. A Selective Review of the Literature on Tactile Sensitivity: 1940-1965. Technical Report AMRL-TR-66-50, Aerospace Medical Research Laboratories, Wright-Patterson AFB OH, April 1966.

24. T. Oomichi, M. Higuchi, A. Okino, N. Kawauchi, Y. Shimizu, A. Maekawa, K. Ohnishi, and T. Hayashi. Intelligent Control of Four Fingered Manipulator System. In *Proc. of the Int. Symp. on Advanced Robot Tech. (ISART)*, page 589. Japan Industrial Robot Association (JIRA) and Advanced Robot Technology Reasearch Association (ARTRA), March 1991.

25. T. Oomichi, A. Maekawa, and T. Hayashi. Multiple Sensory Bilateral Control of A Manipulator With Dexterous Hand. In *The Second Workshop on Manipulators, Sensors and Steps Towards Mobility*, pages 10.1–10.7. University of Salford, England, October 1988.

26. T. Oomichi, T. Miyatake, A. Maekawa, and T. Hayashi. Mechanics and Multiple Sensory Bilateral Control of a Fingered Manipulator. In *Robotics Research: The Fourth Int. Symp.*, pages 145–153, Cambridge, MA, 1988. MIT Press.

27. N. J. M. Patrick, T. B. Sheridan, M. J. Massimino, and B. A. Marcus. Design and Testing of a Non-reactive, Fingertip Tactile Display for Interaction with Remote Environments. Source: Beth Marcus at EXOS, 1991.

28. P. Richard, G. Burdea, and P. Coiffet. Human Performance in Tasks Involving Virtual Objects with Force Feedback. In *Proc. of Interface to Real and Virtual Worlds Conference*, pages 229–238, Montpellier, France, 1993. In French.

29. P. Richard, G. Burdea, D. Gomez, and P. Coiffet. A Comparison of Haptic, Visual and Auditive Force Feedback for Deformable Virtual Objects. In *The Fourth International Conference on Artificial Reality and Tele-Existence (ICAT '94)*, Tokyo, Japan, July 1994.

30. SensAble Devices, Inc. Personal Communication. 225 Court Street, Vanceburg KY, 1993.

31. T. B. Sheridan. *Telerobotics, Automation, and Human Supervisory Control.* MIT Press, 1992.

32. C. E. Sherrick and R. W. Cholewiak. Cutaneous Sensitivity. In K. R. Boff, L. Kaufman, and J. P. Thomas, editors, *Handbook of Human Perception and Performance — Volume I, Sensory Processes and Perception*, pages 12–1 - 12–58. Wiley & Sons, 1986.

33. K. B. Shimoga. Force and Touch Feedback Devices for Dexterous Telemanipulation. In *NASA-CIRSSE Conf. on Intelligent Robotics for Space Exploration*, pages 158–176, Sept/Oct 1992.

34. K. B. Shimoga. Perceptual Feedback Issues in Dexterous Telemanipulation. Technical Report RAL/KBS-2-92, Univ. of Toronto, Robotics & Automation Lab, 1992.

35. M. A. Srinivasan and J. Chen. Human Performance in Controlling Normal Forces of Contact with Rigid Objects. In *ASME Winter Annual Meeting–Session on Haptic Interfaces for Virtual Environment and Teleoperator Systems*, New Orleans, November 1993.

36. H. Z. Tan, M. A. Srinivasan, B. Eberman, and B. Cheng. Human Factors for the Design of Force-Reflecting Haptic Interfaces. In *ASME Winter Annual Meeting–Session on Haptic Interfaces for Virtual Environment and Teleoperator Systems*, Chicago, November 1994.

37. P. Wellman and R. D. Howe. Towards Realistic Vibrotactile Display in Virtual Environments. In *ASME Int. Mech. Eng. Cong. and Exp., DSC-11A*, San Francisco CA, November 1995.

38. G. Westling and R. S. Johansson. Factors Influencing the Force Control During Precision Grip. *Experimental Brain Research*, 53:227–284, 1984.

VITA

[redacted] From 1971 until 1986, I lived in Darien, Connecticut, and graduated from Darien High School in June 1986. I attended Cornell University (Ithaca, NY) on an Air Force ROTC scholarship, graduating with a B.S. in Electrical Engineering. While in college, I worked up to 30 hours per week as an ambulance technician. After entering active duty in January 1991, I attended Bioenvironmental Engineering School at Brooks AFB, Texas, for three and a half months before reporting to the Human Sensory Feedback (HSF) for Telepresence Project, which I now head, in the Bioacoustics Branch of the Armstrong Laboratory (AL/CFBA).

The HSF project focuses on the use of electromechanical systems to display forces and touch sensations from remote and virtual environments to users. The project's efforts are divided into three areas: 1. Coarse manipulation (force feedback to the arms), 2. Fine manipulation (force feedback to the fingers), and 3. Tactile feedback (touch sensations on the fingertips). After some initial work in the fine manipulation area, examining shape-memory alloy actuators for hand exoskeleton use, my experimental work moved into tactile feedback. I performed an engineering characterization of one of our tactile feedback arrays, began publishing basic research on human pattern perception, and designed two virtual surface tactile feedback software programs. The first was used for basic research in pattern perception, and the second gives blind individuals the ability to "see" plotted data on a virtual tactile surface. A patent application has been filed for the latter invention. While working at the lab bench on tactile feedback, I continued my involvement in fine manipulation as an analyst and technology sponsor through the Small Business Innovation Research (SBIR) Program. My analysis culminated in 1995 with the publication of the technical report, "Force-Reflecting Anthropomorphic Hand Masters." As an SBIR technical monitor, I sponsored development of force-reflecting hand masters and component technologies such as novel actuators.

In the evenings I completed coursework towards an M.S. in Electrical Engineering at the University of Dayton, with a concentration in control systems. My master's thesis, "Tactile Feedback for a Force-Reflecting Haptic Display" has fused two areas of our research program (fine manipulation and tactile feedback) and brought me back into empirical work with force reflection. It was completed with support from an In-house Laboratory Independent Research grant from the Air Force Office of Scientific Research.

My spare time is spent with my wife, Sheila, and our animal menagerie. I enjoy breathing compressed air, both SCUBA diving with Sheila and working as an Emergency Medical Technician for Beavercreek Fire Department. Strong medical interests have led me to complete extensive trauma care training, including Advanced Trauma Life Support training while at the Combat Casualty Care Course at Camp Bullis, Texas. Naturally, I am interested in telesurgical and other medical applications of haptic feedback.

PUBLICATIONS

[1] O. D. Brimhall and C. J. Hasser. Magnetostrictive Linear Devices for Force Reflection in Dexterous Telemanipulation. In *Proc. of the North American Conf. on Smart Structures and Materials.* SPIE, February 1994.

[2] C. J. Hasser. Manipulating Molecular Models in "Inner Space" Using a Force-Reflecting Control Arm. Presentation to the Wright Laboratory Symp. on Computational Materials Sci., Wright-Patterson AFB OH, July 1992.

[3] C. J. Hasser. Multi-Element Tactile Feedback for Teleoperation. In *VR Systems '93*, New York NY, October 1993. SIG-Advanced Applications.

[4] C. J. Hasser. Force-Reflecting Anthropomorphic Hand Masters. Technical Report AL/CF-TR-1995-0110, USAF Armstrong Laboratory, Wright-Patterson AFB OH, 1995.

[5] C. J. Hasser. Force-Reflecting Anthropomorphic Handmaster Requirements. In *ASME Int. Mech. Eng. Cong. and Exp., DSC-Vol. 57-2*, San Francisco CA, November 1995.

[6] C. J. Hasser. HAPTAC: A Haptic Tactile Display for the Presentation of Two-Dimensional Virtual or Remote Environments. Technical Report AL/CF-TR-1995-0104, USAF Armstrong Laboratory, Wright-Patterson AFB OH, 1995.

[7] C. J. Hasser. Manipulating Molecular Models in "Inner Space" Using a Force-Reflecting Control Arm. In R. Pachter, B. L. Farmer, and W. W. Adams, editors, *Mini-Symposium on Computational Materials Science Research.* Technical Report WL-TR-95-4008, USAF Wright Laboratory, Wright-Patterson AFB OH, 1995.

[8] C. J. Hasser. Tactile feedback for a force-reflecting haptic display. Master's thesis, University of Dayton, Dayton OH, December 1995.

[9] C. J. Hasser. Unmanned Aerial Vehicle Human Interface in the Twenty-First Century. A New World Vistas Paper for the Air Force Scientific Advisory Board on Human Systems/Biotechnology, June 1995.

[10] C. J. Hasser and E. G. Munday. Shape Memory Alloy Actuators in a Simple Force-Reflecting Teleoperator. Technical Report AL/CF-TR-1993-0163, USAF Armstrong Laboratory, Wright-Patterson AFB OH, July 1992.

[11] C. J. Hasser and J. M. Weisenberger. Preliminary Evaluation of a Shape-Memory Alloy Tactile Feedback Display. In *ASME Winter Annual Meeting–Session on Haptic Interfaces for Virtual Environment and Teleoperator Systems*, pages 73–80, New Orleans LA, November 1993.

[12] C. J. Hasser and J. M. Weisenberger. Shape-Memory Alloy Tactile Feedback Display for Teleoperation and Virtual Reality. *SAFE Journal*, 25(2), April 1995.

[13] E. G. Munday and C. J. Hasser. The Design of a One-Degree-of-Freedom Master-Slave Device Based on a Shape Memory Alloy Actuator. In *Proc. of the 24th Southeastern Symp. on Syst. Theory*, pages 166–170. IEEE Computer Society Press, March 1992.

U. S. Government Printing Office 1996 549-073/40031